

# Comparison of performance of van der Waals-corrected exchange-correlation functionals for interlayer interaction in graphene and hexagonal boron nitride

Irina V. Lebedeva<sup>a,\*</sup>, Alexander V. Lebedev<sup>b</sup>, Andrey M. Popov<sup>c</sup>, Andrey A. Knizhnik<sup>b</sup>

<sup>a</sup>Nano-Bio Spectroscopy Group and ETSF, Universidad del País Vasco, CFM CSIC-UPV/EHU, 20018 San Sebastian, Spain

<sup>b</sup>Kintech Lab Ltd., 3rd Khoroshevskaya Street 12, Moscow 123298, Russia

<sup>c</sup>Institute for Spectroscopy of Russian Academy of Sciences, Troitsk, Moscow 108840, Russia

## Abstract

Exchange-correlation functionals with corrections for van der Waals interactions (PBE-D2, PBE-D3, PBE-D3(BJ), PBE-TS, optPBE-vdW and vdW-DF2) are tested for graphene and hexagonal boron nitride, both in the form of bulk and bilayer. The characteristics of the potential energy surface, such as the barrier to relative sliding of the layers and magnitude of corrugation, and physically measurable properties associated with relative in-plane and out-of-plane motion of the layers including the shear modulus and modulus for axial compression, shear mode frequency and frequency of out-of-plane vibrations are considered. The PBE-D3(BJ) functional gives the best results for the stackings of hexagonal boron nitride and graphite that are known to be ground-state from the experimental studies. However, it fails to describe the order of metastable states of boron nitride in energy. The PBE-D3 and vdW-DF2 functionals, which reproduce this order correctly, are identified as the optimal choice for general studies. The vdW-DF2 functional is preferred for evaluation of the modulus for axial compression and frequency of out-of-plane vibrations, while the PBE-D3 functional is somewhat more accurate in calculations of the shear modulus and shear mode frequency. The best description of the latter properties, however, is achieved also using the vdW-DF2 functional combined with consideration of the experimental interlayer distance. In the specific case of graphene, the PBE-D2 functional works very well and can be further improved by adjustment of the parameters.

**Keywords:** van der Waals interaction, density functional theory, potential energy surface, graphene, hexagonal boron nitride

## 1. Introduction

A number of physical phenomena in two-dimensional bilayers, such as graphene and hexagonal boron nitride, originate from relative displacement of the layers. Relative rotation of the layers gives rise to Moiré patterns [1–3], while static translational displacement is manifested through dislocations in stacking of the layers [4–13]. Dynamic phenomena based on relative motion of the layers include atomic-scale slip-stick motion of a flake attached to a STM tip [14–16], rotation-assisted diffusion and drift of a flake [17, 18] and self-retracting motion of the layers at their telescopic extension [19, 20]. Based on the link between the relative position of the layers and their

electronic properties [21–23] various types of nanosensors [23–27] can be elaborated. Quantitative description of all of these phenomena and devices depends on the characteristics of the potential surface energy of interlayer interaction, i.e. the dependence of interlayer interaction energy on relative in-plane position of the layers.

Direct investigations of the potential energy surface of layered materials are not accessible to modern experimental methods. Nevertheless, there are a number of physical quantities related to interlayer interaction that have been measured experimentally and thus provide some insight into characteristics of the potential energy surface. These quantities include among others shear modulus [28–32] and modulus for axial compression [28, 29, 33–36], shear mode frequency ( $E_{2g}$  mode with adjacent layers sliding rigidly in the opposite in-plane directions) [29, 32, 37–39, 39, 40], frequency of relative out-of-plane vibrations ( $B_{1g}$  ZO mode with adjacent layers sliding rigidly towards and away from each other) [29, 36–38, 41, 42] and width

\*Corresponding author

Email addresses: liv\_ira@hotmail.com (Irina V. Lebedeva), alexandrleb@gmail.com (Alexander V. Lebedev), popov-isana@mail.ru (Andrey M. Popov), knizhnik@kintechlab.com (Andrey A. Knizhnik)

of dislocations in stacking [4, 7, 8].

Along with these experimental investigations of the properties related to interlayer interaction, significant advances have been achieved in their theoretical description. Semi-empirical potentials for interaction of various two-dimensional layers have been developed, including among others the potentials for graphene [43, 44], boron nitride [45] and graphene-boron nitride heterostructure [46]. The registry index surface was introduced to analyze qualitative features of the potential surface of interlayer interaction energy in hexagonal boron nitride bilayer [47] and graphene-boron nitride heterostructure [46, 48, 49]. Simple approximations of the potential energy surfaces at a given interlayer distance containing only the first components of Fourier expansions were proposed on the basis of symmetry considerations for bilayer graphene [44, 50–53], boron nitride [53, 54] and graphene-boron nitride heterostructure [53]. These expressions were also extended to take into account the dependence of corrugations of the potential energy surface on the interlayer distance [53, 55].

The approximations of the potential energy surface using the first Fourier components include only one energy parameter for graphene [44, 50–52] and boron nitride with the layers aligned in the same direction [54] and two energy parameters for boron nitride with the layers aligned in the opposite directions [54]. This implies that all physical properties characterising the potential energy surface at a given interlayer distance are interrelated. In this way the barrier to relative motion of the layers in graphene bilayer was estimated using the experimental data on the shear mode frequency [51] and width of dislocations in stacking [4]. In spite of success of such semi-empirical developments, it should, nevertheless, be kept in mind that they all have been derived or tested on the basis of first-principles calculations and rely on their accuracy.

The interaction of two-dimensional layers in materials, such as graphene and hexagonal boron nitride, is, however, of long-range van der Waals (vdW) nature and this leads to breakdown of otherwise accurate density functional theory (DFT) methods. Several ways to include description of long-range vdW interactions have been considered. The most straightforward one is just to add the corresponding semi-empirical term [56–59]. Attempts to include the vdW interactions on the fully first-principles footing have been also made through the density-density interaction term describing nonlocal correlations within the long-range correlation function [60–62].

In the present paper we address the accuracy of these

DFT methods for graphene and hexagonal boron nitride by comparison of the calculation results with the experimentally measurable quantities. The performance of different DFT methods for description of vdW interlayer interactions has been already addressed in papers [53, 55, 63, 64]. However, paper [63] was limited to consideration of the properties of graphite related only to changes in the interlayer distance but not to in-plane displacement of the layers. In paper [53], the performance of only two DFT methods, DFT-D2 and vdW-DF2, was compared to the random phase approximation (RPA) data. In papers [55, 64], the authors studied only the characteristics of the potential energy surfaces of hexagonal boron nitride [64] and graphene [55] without relation to any directly measurable quantities. In the present paper, we pay attention both to the properties characterizing out-of-plane motion of the layers, such as the frequency of relative out-of-plane vibrations and modulus for axial compression, which are relevant in systems under external load, as well as the properties associated with in-plane displacement of the layers, such as the shear modulus and shear mode frequency, which are important for lubricity and development of nanoelectromechanical devices based on relative sliding of the layers. Furthermore, the performance of the same exchange-correlation functionals with account of vdW interactions is correlated for two key materials in nanotechnology, graphene and hexagonal boron nitride. The comparison with the *ab initio* methods that adequately describe vdW interactions, such as RPA [53, 65], local second-order Møller-Plesset perturbation theory (LMP2) [64] and quantum Monte Carlo (QMC) [66, 67], is made along with the reference to the experimental data.

The paper is organized as follows. In section 2 the calculation parameters and considered methods for description of vdW interactions are described. In section 3 the results of calculations for graphene and hexagonal boron nitride are presented and the accuracy of the vdW-corrected exchange-correlation functionals is discussed. Finally the conclusions are summarized.

## 2. Methodology

The DFT calculations have been performed using VASP code [68] for the maximum kinetic energy of 600 eV. The projector augmented-wave method [69] is used to describe the interaction of valence electrons. The convergence threshold of the self-consistent field is  $10^{-8}$  eV. The rectangular unit cell including 4 atoms in each layer is considered under periodic boundary conditions. The height of the simulation cell is 20 Å for bilayers and is equal to the doubled

interlayer distance for bulk materials. The Monkhorst-Pack method [70] is used to perform the integration over the Brillouin zone. The k-point grid is  $24 \times 36 \times 1$  for bilayers and  $24 \times 36 \times 18$  for bulk (here and below axes  $x$  and  $y$  are chosen in the armchair and zigzag directions, respectively). Convergence studies carried out previously for graphene bilayer and graphite [44] showed that these parameters allow to converge the properties of the potential energy surface within the accuracy of 2%.

The bond length has been optimized for single-layer graphene and boron nitride using the exchange-correlation functional of Perdew, Burke and Ernzerhof (PBE) [71] without inclusion of vdW interactions. The corresponding value for graphene is  $l = 1.425 \text{ \AA}$ , close to the experimental data for graphite [28, 40, 72–77] and the results of previous calculations [43, 44, 50, 55, 60, 78]. For boron nitride, the optimized bond length is  $l = 1.451 \text{ \AA}$ , in agreement with the experimental data for bulk boron nitride [79–87] and the results of first-principles calculations [64, 88–99]. The effect of interlayer interaction on the structure of the layers is neglected [64].

The following approaches for description of vdW interactions within DFT are considered: DFT-D2 [56], DFT-D3 [57], DFT-D3(BJ) [58], DFT-TS [59], optPBE-vdW [62] and vdW-DF2 [61].

In the DFT-D approach [56–58], the total energy  $E_{DFT-D}$  is calculated as the sum of the standard Kohn-Sham energy  $E_{KS-DFT}$  and the semi-empirical dispersion correction  $E_{\text{disp}}$ , so that  $E_{DFT-D} = E_{KS-DFT} + E_{\text{disp}}$ . The general form of the dispersion term is

$$E_{\text{disp}} = -\frac{1}{2} \sum_{A \neq B} \sum_{n=6,8,\dots} s_n \frac{C_n^{AB}}{R_{AB}^n} f_{\text{dmp},n}(R_{AB}), \quad (1)$$

where  $C_n^{AB}$  is the  $n$ -th order dispersion coefficient for the pair of atoms  $A$  and  $B$ ,  $R_{AB}$  is their internuclear distance,  $s_n$  is the global scaling factor depending on the exchange-correlation functional used and  $f_{\text{dmp},n}$  is the damping function serving to avoid singularities at small  $R_{AB}$  and double-counting effects of electron correlation at intermediate distances.

In the DFT-D2 method [56], only  $n = 6$  terms are included. The damping function  $f_{\text{dmp},6}$  has the form of

$$f_{\text{dmp},6}(R_{AB}) = \frac{1}{1 + e^{-d(R_{AB}/R_0^{AB}-1)}}, \quad (2)$$

where  $R_0^{AB}$  is the sum of atomic vdW radii and  $d = 20$ . The  $C_6^A$  coefficients for different atoms  $A$  are derived on the basis of atomic polarization potentials and static dipole polarizabilities from the PBE0 calculations [100]. The geometric mean rule is applied to estimate  $C_6^{AB}$  coefficients

for pairs of distinct elements  $C_6^{AB} = \sqrt{C_6^A C_6^B}$ . The scaling factor  $s_6 = 0.75$  is used for the PBE functional.

In the DFT-D3 approach [57],  $n = 6$  and  $n = 8$  terms are considered. The damping function  $f_{\text{dmp},n}$  has the form of

$$f_{\text{dmp},n}(R_{AB}) = \frac{1}{1 + 6(R_{AB}/(s_{r,n}R_0^{AB}))^{-\alpha_n}}, \quad (3)$$

where  $s_{r,6}$  is the scaling factor of the cutoff radius  $R_0^{AB}$  dependent on the exchange-correlation functional used and parameters  $s_{r,8}$ ,  $\alpha_6$  and  $\alpha_8$  are fixed at values 1, 14 and 16, respectively. The dispersion coefficients are obtained from the Casimir-Polder formula [101]

$$C_6^{AB} = \frac{3}{\pi} \int_0^\infty d\omega \frac{1}{m} \left[ \alpha^{A_m H_p}(i\omega) - \frac{p}{2} \alpha^{H_2}(i\omega) \right] \times \frac{1}{k} \left[ \alpha^{B_k H_l}(i\omega) - \frac{l}{2} \alpha^{H_2}(i\omega) \right] \quad (4)$$

modified to use polarizabilities  $\alpha^M$  of simple molecules  $M = A_m H_p$ ,  $B_k H_l$  and  $H_2$  with well-defined electronic structure. In this way, the use of free-atom polarizabilities, which can be strongly influenced by energetically low-lying atomic states, is avoided and the dispersion coefficients dependent on the coordination number of the atoms are introduced. The  $C_8^{AB}$  coefficients are computed from  $C_6^{AB}$  coefficients on the basis of the power series expansion of dispersion forces (see Ref. [57] and references therein).

In the DFT-D3(BJ) approach [58], the Becke-Jonson (BJ) damping is used

$$f_{\text{dmp},n}(R_{AB}) = \frac{R_{AB}^n}{R_{AB}^n + (a_1 R_0^{AB} + a_2)^n}, \quad (5)$$

where  $a_1$  and  $a_2$  are adjustable parameters. Furthermore, in this method  $R_0^{AB} = \sqrt{C_8^{AB}/C_6^{AB}}$ .

The Tkatchenko-Scheffler DFT-TS approach [59] is based on the same formal expressions as DFT-D2. However, in this case the dispersion coefficients and damping function depend on the charge density to take into account the effects of local chemical environment of atoms. The dispersion coefficient  $C_6^{A,\text{free}}$  and vdW radius  $R_0^{A,\text{free}}$  of free atom  $A$  are scaled for atoms in molecules as  $C_6^A = (V_{\text{eff}}^A/V_{\text{free}}^A)^2 C_6^{A,\text{free}}$  and  $R_0^A = (V_{\text{eff}}^A/V_{\text{free}}^A)^{1/3} R_0^{A,\text{free}}$ , where the ratio  $V_{\text{eff}}^A/V_{\text{free}}^A$  between the effective and free atomic volumes is determined from the Hirshfeld partitioning of the all-electron density. The dispersion coefficients for pairs of atoms are found as

$$C_6^{AB} = \frac{2C_6^A C_6^B}{\frac{\alpha_0^B}{\alpha_0^A} C_6^A + \frac{\alpha_0^A}{\alpha_0^B} C_6^B}, \quad (6)$$

where  $\alpha_0^A$  and  $\alpha_0^B$  are the static polarizabilities.

Due to the poor performance of the DFT-TS approach for ionic solids in the case of boron nitride we also consider the extension of this method DFT-TS/HI [102, 103] using iterative Hirshfeld partitioning on the basis of the scheme proposed by Bultinck [104]. In this iterative Hirshfeld algorithm, the neutral reference atoms are replaced by ions with fractional charges determined along with effective atomic volumes at each iteration step. For boron nitride, we also test the DFT-TS+SCS approach [105] in which screening of the electrostatic interaction between dipoles by the polarizable surrounding is taken into account. Since we do not observe significant improvement in description of properties of boron nitride when using the DFT-TS/HI and DFT-TS+SCS methods compared to DFT-TS (see section 3), only the DFT-TS approach is considered for graphene bilayer and graphite.

The optPBE-vdW [62] and vdW-DF2 [61] approaches are based on the vdW-DF non-local correlation functional [60] in which vdW interactions are taken into account through the density-density interaction term. In the optPBE-vdW functional, the exchange part is optimized for the vdW-DF correlation part on the basis of the S22 benchmark set of weakly interacting dimers and for water clusters [62]. In the vdW-DF2 functional [61], the use of the more accurate exchange functional is supplemented by application of the large-N asymptote gradient correction in the vdW kernel. An overview of the performance of these approaches for solids in VASP can be found in [106].

### 3. Results

To compare performance of different methods for description of vdW interactions in graphene and hexagonal boron nitride we have carried out calculations for a series of properties related to out-of-plane and in-plane displacements of the layers (Tables 1 – 6). The basic properties associated with relative position of the layers are the equilibrium interlayer distance  $d_{\text{eq}}$  and binding energy. The out-of-plane motion of the layers is characterized by the frequency  $f_B$  of out-of-plane vibrations of the layers and modulus  $C_{33}$  for axial compression. As the experimentally measurable properties related to in-plane motion we consider the frequency  $f_E$  of in-plane vibrations and shear modulus  $C_{44}$ . We also calculate relative energies of symmetric stackings of the layers at a given interlayer distance. Though such energies cannot be easily measured, there is the experimental evidence for the ground-state

and metastable stackings and some indirect estimates are available.

#### 3.1. Interlayer distance and binding energy

The interlayer distance is known with high precision for bulk materials [28, 40, 73, 76, 77, 79, 80, 84–87, 117, 118] (Tables 2 and 6). Since the energy calculations are performed at zero temperature, we consider as the reference for graphite the value of 3.336 Å corresponding to 4.2 K [73] and for boron nitride the value of 3.301 Å corresponding to 10 K [84]. It should be noted, however, that increasing the temperature up to the room one does not lead to drastic changes in the interlayer distance and it grows only up to 3.36 Å for graphite [28, 40, 76, 77] and to 3.33 Å for boron nitride [79, 80, 84–87, 117, 118].

Very close to the room-temperature interlayer distance in graphite is the value of 3.35 Å obtained for bilayer and trilayer graphene on copper [5] (Table 1). Somewhat larger interlayer distances of 3.37–3.49 Å were measured for few-layer graphene on silicon carbide [107, 108] and nickel [109]. These increased values can be explained by strong interaction of the corresponding substrates with graphene. To avoid consideration of such effects we use as the reference value for graphene bilayer the result from paper [5]. The interlayer distances of  $3.25 \pm 0.10$  Å [115] and  $\sim 3.5$  Å [88, 116] measured for 10–20 layers of boron nitride are on the order of those for bulk. However, the low accuracy of these data makes impossible their consideration as reference values.

All the considered exchange-correlation functionals with account of vdW interactions give the equilibrium interlayer distances for graphene bilayer, graphite and bulk boron nitride within the relative deviation of 7% from the reference values (Tables 1, 2 and 6). Though this deviation is rather small, as discussed later, it is critical for prediction of properties of graphene and boron nitride layers associated with their relative motion.

The experimental data on the binding energy in graphene-like materials are rather diverse, ranging from  $-31$  meV/atom to  $-52$  meV/atom [111–114] (note that all energies for bilayers in the present paper are given in meV per atom in the upper (adsorbed) layer). The QMC [66, 67] and RPA approaches [65] gave similar results in the range from  $-36$  meV/atom to  $-52$  meV/atom [65–67] (except for the recent RPA value of  $-91$  meV/atom [53]). Therefore, as the reference value in the case we take the average of the experimental values. However, it should be kept in mind that the real binding energy lies within 40% interval around this value. The considered functionals with account of vdW interactions give the binding en-

Table 1: Properties of graphene bilayer (equilibrium interlayer distance  $d_{\text{eq}}$ , binding energy in the AB stacking  $E_{\text{AB}}$ , magnitude of corrugation of the potential energy surface  $\Delta E_{\text{AA}} = E_{\text{AA}} - E_{\text{AB}}$ , barrier to relative sliding of the layers  $\Delta E_{\text{SP}} = E_{\text{SP}} - E_{\text{AB}}$ , shear modulus  $C_{44}$ , modulus for axial compression  $C_{33}$ , frequencies of relative in-plane and out-of-plane vibrations  $f_E$  and  $f_B$ , respectively) calculated using different functionals. The data for the experimental interlayer distance  $d_{\text{exp}} = 3.34 \text{ \AA}$  are also given.

Approach	$d_{\text{eq}}$ ( $\text{\AA}$ )	$E_{\text{AB}}$ (meV/atom)	$\Delta E_{\text{AA}}$ (meV/atom)	$\Delta E_{\text{SP}}$ (meV/atom)	$C_{44}$ (GPa)	$C_{33}$ (GPa)	$f_E$ ( $\text{cm}^{-1}$ )	$f_B$ ( $\text{cm}^{-1}$ )	Ref.
PBE-D2	3.256	-50.41	19.20	2.04	4.99	38.35	33.78	93.69	This work
PBE-D3	3.530	-44.03	7.25	0.75	1.89	22.89	20.82	69.51	This work
PBE-D3(BJ)	3.410	-48.55	11.48	1.23	3.12	30.70	26.13	81.91	This work
PBE-TS	3.360	-73.05	15.30	1.88	4.59	62.40	31.90	117.6	This work
optPBE-vdW	3.465	-59.97	9.71	1.04	2.67	31.39	23.97	82.15	This work
vdW-DF2	3.544	-49.11	7.33	0.77	2.07	31.73	20.84	81.68	This work
PBE-D2 corrected	3.319	-42.674	15.62	1.67	4.09	33.35	29.79	85.09	This work
PBE ( $d = d_{\text{exp}}$ )			14.50	1.58	3.86		29.35		This work
PBE-D2 ( $d = d_{\text{exp}}$ )			14.49	1.55	3.82		29.18		This work
PBE-D3 ( $d = d_{\text{exp}}$ )			14.38	1.60	3.91		29.55		This work
PBE-D3(BJ) ( $d = d_{\text{exp}}$ )			14.57	1.58	3.91		29.54		This work
PBE-TS ( $d = d_{\text{exp}}$ )			16.31	2.01	4.89		33.02		This work
optPBE-vdW ( $d = d_{\text{exp}}$ )			14.86	1.62	3.96		29.71		This work
vdW-DF2 ( $d = d_{\text{exp}}$ )			14.73	1.62	3.84		29.29		This work
LDA	3.33	-24.2	9.9	1.3					[55]
LDA	3.33	-22.8	9.57	1.82					[78]
PBE-D2	3.31	-43.1	9.9	1.3					[55]
PBE-D2	3.25	-50.6	19.5	2.07					[44]
PBE-D2	3.25	-50.52	12.32	1.95		38			[53]
vdW-DF	3.62	-49.9	5.8	0.5					[55]
vdW-DF	3.35	-29.3	18.9	1.92					[44]
vdW-DF2	3.55	-49.02	5.75	0.62		30			[53]
QMC	$3.43 \pm 0.04$	$-35.6 \pm 1.6$	$\sim 12.4$					$83 \pm 7$	[66]
RPA	3.39	-91.35	8.81	1.53		30			[53]
Exp. 2-3 layers/Cu	3.35								[5]
Exp. 4 layers/SiC	$3.37 - 3.46 \pm 0.25$								[107]
Exp. 9 layers/SiC	$3.370 \pm 0.005$								[108]
Exp. $\leq 44$ layers/Ni	$3.478 - 3.490$								[109]
Exp. $\leq 12$ layers/SiO <sub>2</sub> /Si	$\sim 3.7$								[110]
Exp.							$28 \pm 3$		[39]
Exp.							32		[32]
Exp.								$80 \pm 2$	[41]
Exp.								81	[42]
Reference values	3.35						30	80.5	

Table 2: Properties of graphite (equilibrium interlayer distance  $d_{\text{eq}}$ , binding energy in the AB stacking  $E_{\text{AB}}$ , magnitude of corrugation of the potential energy surface  $\Delta E_{\text{AA}} = E_{\text{AA}} - E_{\text{AB}}$ , barrier to relative sliding of the layers  $\Delta E_{\text{SP}} = E_{\text{SP}} - E_{\text{AB}}$ , shear modulus  $C_{44}$ , modulus for axial compression  $C_{33}$ , frequencies of relative in-plane and out-of-plane vibrations  $f_E$  and  $f_B$ , respectively) calculated using different functionals. The data for the experimental interlayer distance  $d_{\text{exp}} = 3.34 \text{ \AA}$  are also given.

Approach	$d_{\text{eq}}$ ( $\text{\AA}$ )	$E_{\text{AB}}$ (meV/atom)	$\Delta E_{\text{AA}}$ (meV/atom)	$\Delta E_{\text{SP}}$ (meV/atom)	$C_{44}$ (GPa)	$C_{33}$ (GPa)	$f_E$ ( $\text{cm}^{-1}$ )	$f_B$ ( $\text{cm}^{-1}$ )	Ref.
PBE-D2	3.223	-55.61	20.42	2.35	5.38	42.24	49.89	139.8	This work
PBE-D3	3.485	-48.13	8.35	0.92	2.35	24.91	31.73	103.2	This work
PBE-D3(BJ)	3.374	-53.15	12.46	1.41	3.48	32.13	39.18	119.1	This work
PBE-TS	3.332	-82.54	16.26	2.12	4.76	68.15	46.16	174.6	This work
optPBE-vdW	3.442	-64.28	10.29	1.15	2.78	32.84	35.33	119.2	This work
vdW-DF2	3.521	-52.37	7.89	0.87	2.22	33.30	30.69	118.7	This work
PBE-D2 corrected	3.290	-46.91	16.50	1.87	4.29	37.13	44.10	129.69	This work
PBE ( $d = d_{\text{exp}}$ )			13.88	1.58	3.61		40.16		This work
PBE-D2 ( $d = d_{\text{exp}}$ )			13.88	1.57	3.58		39.95		This work
PBE-D3 ( $d = d_{\text{exp}}$ )			13.74	1.61	3.66		40.39		This work
PBE-D3(BJ) ( $d = d_{\text{exp}}$ )			13.96	1.59	3.63		40.25		This work
PBE-TS ( $d = d_{\text{exp}}$ )			15.89	2.07	4.70		45.79		This work
optPBE-vdW ( $d = d_{\text{exp}}$ )			14.38	1.65	3.71		40.68		This work
vdW-DF2 ( $d = d_{\text{exp}}$ )			14.26	1.64	3.60		40.10		This work
LDA, GGA ( $d = d_{\text{exp}}$ )			15	$\sim 1$					[43]
QMC	$3.426 \pm 0.036$	$-56 \pm 6$							[67]
RPA	3.34	-48				36			[65]
Exp. 4.2 K	$3.3360 \pm 0.0005$								[73]
Exp. 297 K	$3.3538 \pm 0.0005$								[73]
Exp. $275 \pm 2$ K	3.354								[77]
Exp. $\sim 300$ K	3.356								[76]
Exp. $\sim 300$ K	3.356				$5.0 \pm 0.3$	$38.7 \pm 0.7$			[28]
Exp. $\sim 300$ K	$3.353 \pm 0.002$						$44 \pm 1$		[40]
Exp.		$-52 \pm 5$							[111]
Exp.		$-43 \pm 5$							[112]
Exp.		$-35 (+15, -10)$							[113]
Exp.		$-31 \pm 2$							[114]
Exp.					$4.6 \pm 0.2$	$37.1 \pm 0.5$	45	$\sim 130$	[29]
Exp.					4.3		44		[32]
Exp.					$5.05 \pm 0.35$				[30]
Exp.					$4.0 \pm 0.4$				[31]
Exp.						$36.5 \pm 1.0$			[33]
Exp.						40.7			[34]
Exp.						$36.6 \pm 0.1$			[35]
Exp.						$34.0 \pm 0.2$		127	[36]
Exp.							42	127	[37, 38]
Exp.							44		[39]
Exp.								132.3	[41]
Reference values	3.336	-40.3			4.59	37.3	43.5	129	

Table 3: Energies of symmetric stackings of hexagonal boron nitride bilayer (for the layers aligned in the opposite directions: equilibrium interlayer distance  $d_{\text{eq}}$ , binding energy in the AA' stacking  $E_{AA'}$ , relative energy of the AB1' stacking  $E_{AB1'} = E_{AB1'} - E_{AA'}$ , magnitude of corrugation of the potential energy surfaces  $\Delta E_{AB2'} = E_{AB2'} - E_{AA'}$ , barriers to relative sliding of the layers  $\Delta E_{SP'} = E_{SP'} - E_{AA'}$ ; for the layers aligned in the same direction: relative energy of the AB stacking  $\Delta E_{AB} = E_{AB} - E_{AA'}$ , magnitude of corrugation of the potential energy surface  $\Delta E_{AA} = E_{AA} - E_{AB}$ , barrier to relative sliding of the layers  $\Delta E_{SP} = E_{SP} - E_{AB}$ ) calculated using different functionals. The data for the experimental interlayer distance  $d_{\text{exp}} = 3.30 \text{ \AA}$  are also given.

Approach	$d_{\text{eq}}$ (Å)	$E_{AA'}$ (meV/atom)	$E_{AB1'}$ (meV/atom)	$\Delta E_{AB2'}$ (meV/atom)	$\Delta E_{SP'}$ (meV/atom)	$\Delta E_{AB}$ (meV/atom)	$\Delta E_{AA}$ (meV/atom)	$\Delta E_{SP}$ (meV/atom)	Ref.
PBE-D2	3.120	-68.77	3.39	26.86	4.70	-1.39	35.10	3.58	This work
PBE-D3	3.438	-44.04	2.21	10.82	2.50	0.08	12.89	1.39	This work
PBE-D3(BJ)	3.360	-46.64	1.55	13.14	2.28	-0.29	15.72	1.70	This work
PBE-TS	3.368	-75.89	-0.69	10.61	0.98	-1.76	15.39	1.81	This work
PBE-TS/HI	3.474	-52.02	0.08	6.06	0.98	-0.68	8.25	1.14	This work
PBE-TS+SCS	3.411	-103.98	8.62	17.83	8.62	2.41	19.26	2.06	This work
optPBE-vdW	3.416	-59.75	1.86	11.70	2.35	0.05	13.53	1.48	This work
vdW-DF2	3.502	-48.42	2.36	9.553	2.54	0.58	10.26	1.13	This work
PBE ( $d = d_{\text{exp}}$ )			1.83	15.94	2.74	-0.35	19.04	2.05	This work
PBE-D2 ( $d = d_{\text{exp}}$ )			2.15	15.91	2.90	-0.32	19.24	2.03	This work
PBE-D3 ( $d = d_{\text{exp}}$ )			2.92	16.47	3.46	-0.05	19.77	2.10	This work
PBE-D3(BJ) ( $d = d_{\text{exp}}$ )			1.74	15.87	2.67	-0.41	19.07	2.05	This work
PBE-TS ( $d = d_{\text{exp}}$ )			-1.87	13.57	0.84	-2.08	18.24	2.05	This work
PBE-TS/HI ( $d = d_{\text{exp}}$ )			-0.71	13.38	1.62	-1.60	17.68	2.32	This work
PBE-TS+SCS ( $d = d_{\text{exp}}$ )			11.82	23.89	11.82	2.82	27.41	2.93	This work
optPBE-vdW ( $d = d_{\text{exp}}$ )			2.29	16.64	3.11	-0.15	19.59	2.13	This work
vdW-DF2 ( $d = d_{\text{exp}}$ )			3.32	17.34	3.90	0.39	19.74	2.17	This work
PBEsol ( $d = d_{\text{exp}}$ )			1.45	16.06	2.51	-0.56	19.43	2.08	This work
PBEsol-D3 ( $d = d_{\text{exp}}$ )			1.87	15.67	2.74	-0.58	19.52	2.11	This work
PBEsol-D3(BJ) ( $d = d_{\text{exp}}$ )			1.50	16.09	2.55	-0.53	19.42	2.08	This work
rPBE ( $d = d_{\text{exp}}$ )			2.01	15.78	2.84	-0.23	18.70	2.02	This work
rPBE-D3 ( $d = d_{\text{exp}}$ )			2.76	15.49	3.31	-0.32	19.43	2.10	This work
rPBE-D3(BJ) ( $d = d_{\text{exp}}$ )			2.13	16.00	2.94	-0.06	18.52	1.99	This work
revPBE ( $d = d_{\text{exp}}$ )			1.97	15.85	2.82	-0.25	18.79	2.02	This work
revPBE-D3 ( $d = d_{\text{exp}}$ )			2.31	15.01	2.95	-0.64	19.48	2.11	This work
revPBE-D3(BJ) ( $d = d_{\text{exp}}$ )			1.80	15.50	2.69	-0.47	18.94	2.04	This work
PBE0 ( $d = d_{\text{exp}}$ )			3.51	18.19		0.20	21.19	2.31	This work
LMP2	3.34		4.42	16.50	3.4	0.24	19.45	~ 2.4	[64]
PBEsol	3.33		3.30	14.94		0.30	16.92	~ 1.8	[64]
HF	3.33		8.20	21.82		1.86	23.88	~ 2.7	[64]
PBE-D	3.127		7.90	26.16		0.10	33.50	~ 3.0	[64]
PBE0-D	2.987		11.38	39.76		-2.22	57.08	~ 5.4	[64]
PBE ( $d = 3.34 \text{ \AA}$ )			3.04	14.08		0.26	15.96	~ 2.0	[64]
PBE0 ( $d = 3.34 \text{ \AA}$ )			4.52	16.16		0.76	17.88	~ 1.8	[64]
PBE-D ( $d = 3.34 \text{ \AA}$ )			3.4	14.12		0.34	16.12	~ 1.9	[64]
PBE0-D ( $d = 3.34 \text{ \AA}$ )			4.88	16.20		0.92	17.96	~ 1.8	[64]
PBE-D2	3.12	-68.53	3.24	19.11	~ 4.4	-1.17	22.75	3.78	[53]
vdW-DF2	3.51	-50.05	2.40	7.41	> 2.4	0.68	7.41	1.03	[53]
RPA	3.34	-37.62	3.57	11.04	> 3.7	0.76	11.40	2.06	[53]

Table 4: Properties of hexagonal boron nitride bilayer (for the layers aligned in the opposite directions: equilibrium interlayer distance  $d_{\text{eq}}$ , shear modulus  $C_{44}$ , modulus for axial compression  $C_{33}$ , frequencies of relative in-plane and out-of-plane vibrations  $f_E$  and  $f_B$ , respectively; for the layers aligned in the same direction: shear modulus  $C'_{44}$  and frequency of relative in-plane vibrations  $f'_E$ ) calculated using different functionals. The data for the experimental interlayer distance  $d_{\text{exp}} = 3.30 \text{ \AA}$  are also given.

Approach	$d_{\text{eq}}$ ( $\text{\AA}$ )	$C_{44}$ (GPa)	$C_{33}$ (GPa)	$f_E$ ( $\text{cm}^{-1}$ )	$f_B$ ( $\text{cm}^{-1}$ )	$C'_{44}$ (GPa)	$f'_E$ ( $\text{cm}^{-1}$ )	Ref.
PBE-D2	3.120	7.42	58.60	42.17	118.46	8.22	44.38	This work
PBE-D3	3.438	3.58	26.18	27.90	75.42	3.47	27.44	This work
PBE-D3(BJ)	3.360	3.97	27.16	29.73	77.71	4.14	30.33	This work
PBE-TS	3.368	2.92	45.40	25.47	100.35	4.25	30.70	This work
PBE-TS/HI	3.474		26.55		75.56			This work
PBE-TS+SCS	3.411	7.27	42.04	39.91	95.96	5.12	33.50	This work
optPBE-vdW	3.416	3.72	29.67	28.54	80.56	3.64	28.21	This work
vdW-DF2	3.502	3.32	32.80	26.61	83.66	2.81	24.50	This work
PBE ( $d = d_{\text{exp}}$ )		4.93		33.40		4.66	32.49	This work
PBE-D2 ( $d = d_{\text{exp}}$ )		4.74		32.77		4.90	33.30	This work
PBE-D3 ( $d = d_{\text{exp}}$ )		5.12		34.04		5.05	33.83	This work
PBE-D3(BJ) ( $d = d_{\text{exp}}$ )		4.70		32.63		4.93	33.40	This work
PBE-TS ( $d = d_{\text{exp}}$ )		3.18		26.83		4.74	32.78	This work
PBE-TS+SCS ( $d = d_{\text{exp}}$ )		9.72		46.91		7.11	40.14	This work
optPBE-vdW ( $d = d_{\text{exp}}$ )		5.08		33.93		5.06	33.84	This work
vdW-DF2 ( $d = d_{\text{exp}}$ )		5.18		34.25		5.56	35.50	This work
PBE-D2	3.12		55					[53]
vdW-DF2	3.51		24					[53]
RPA	3.34		46					[53]
Exp. 10 layers	$3.25 \pm 0.10$							[115]
Exp. $\leq 20$ layers	$\sim 3.5$							[116]
Exp. $\leq 14$ layers	$\sim 3.5$							[88]



Table 5: Energies of symmetric stackings of hexagonal boron nitride bulk (for the layers aligned in the opposite directions: equilibrium interlayer distance  $d_{\text{eq}}$ , binding energy in the AA' stacking  $E_{AA'}$ , relative energy of the AB1' stacking  $\Delta E_{AB1'} = E_{AB1'} - E_{AA'}$ , magnitude of corrugation of the potential energy surfaces  $\Delta E_{AB2'} = E_{AB2'} - E_{AA'}$ , barriers to relative sliding of the layers  $\Delta E_{SP'} = E_{SP'} - E_{AA'}$ ; for the layers aligned in the same direction: relative energy of the AB stacking  $\Delta E_{AB} = E_{AB} - E_{AA'}$ , magnitude of corrugation of the potential energy surface  $\Delta E_{AA} = E_{AA} - E_{AB}$ , barrier to relative sliding of the layers  $\Delta E_{SP} = E_{SP} - E_{AB}$ ) calculated using different functionals. The data for the experimental interlayer distance  $d_{\text{exp}} = 3.30 \text{ \AA}$  are also given.

Approach	$d_{\text{eq}}$ (Å)	$E_{AA'}$ (meV/atom)	$E_{AB1'}$ (meV/atom)	$\Delta E_{AB2'}$ (meV/atom)	$\Delta E_{SP'}$ (meV/atom)	$\Delta E_{AB}$ (meV/atom)	$\Delta E_{AA}$ (meV/atom)	$\Delta E_{SP}$ (meV/atom)	Ref.
PBE-D2	3.088	-76.66	4.08	30.04	5.61	-1.37	39.48	4.16	This work
PBE-D3	3.398	-48.31	2.52	12.34	2.85	0.12	14.68	1.60	This work
PBE-D3(BJ)	3.318	-51.35	1.78	15.12	2.67	-0.28	18.05	1.99	This work
PBE-TS	3.317	-86.48	-2.53	13.00	0.63	-1.98	16.84	1.86	This work
PBE-TS/HI	3.386	-61.15	-0.46	10.19	1.33	-1.17	13.39	1.82	This work
PBE-TS+SCS	3.326	-72.30	-2.07	13.53	0.66	-1.11	15.19	1.45	This work
optPBE-vdW	3.388	-64.61	1.89	12.82	2.49	-0.02	14.96	1.66	This work
vdW-DF2	3.478	-52.09	2.36	10.30	2.61	0.52	11.25	1.25	This work
PBE ( $d = d_{\text{exp}}$ )			1.95	16.10	2.87	-0.24	19.12	2.10	This work
PBE-D2 ( $d = d_{\text{exp}}$ )			2.28	16.07	3.03	-0.22	19.33	2.09	This work
PBE-D3 ( $d = d_{\text{exp}}$ )			3.04	16.63	3.60	0.05	19.86	2.16	This work
PBE-D3(BJ) ( $d = d_{\text{exp}}$ )			1.86	16.02	2.81	-0.31	19.15	2.11	This work
PBE-TS ( $d = d_{\text{exp}}$ )			-2.82	13.91	0.63	-2.02	17.60	1.907	This work
PBE-TS/HI ( $d = d_{\text{exp}}$ )			-0.66	14.82	1.71	-1.55	19.08	2.36	This work
PBE-TS+SCS ( $d = d_{\text{exp}}$ )			-2.61	14.58	0.63	-1.26	16.19	1.52	This work
optPBE-vdW ( $d = d_{\text{exp}}$ )			2.26	16.79	3.15	-0.15	19.83	2.20	This work
vdW-DF2 ( $d = d_{\text{exp}}$ )			3.24	17.51	3.90	0.37	20.02	2.25	This work
PBEsol ( $d = d_{\text{exp}}$ )			1.60	16.20	2.67	-0.44	19.48	2.14	This work
PBEsol-D3 ( $d = d_{\text{exp}}$ )			2.02	15.80	2.89	-0.46	19.57	2.17	This work
PBEsol-D3(BJ) ( $d = d_{\text{exp}}$ )			1.65	16.23	2.70	-0.41	19.47	2.14	This work
rPBE ( $d = d_{\text{exp}}$ )			2.11	15.96	2.96	-0.14	18.82	2.07	This work
rPBE-D3 ( $d = d_{\text{exp}}$ )			2.86	15.67	3.42	-0.23	19.55	2.15	This work
rPBE-D3(BJ) ( $d = d_{\text{exp}}$ )			2.23	16.18	3.06	0.03	18.64	2.05	This work
revPBE ( $d = d_{\text{exp}}$ )			2.07	16.02	2.95	-0.16	18.90	2.08	This work
revPBE-D3 ( $d = d_{\text{exp}}$ )			2.42	15.18	3.07	-0.55	19.59	2.16	This work
revPBE-D3(BJ) ( $d = d_{\text{exp}}$ )			1.91	15.67	2.81	-0.38	19.05	2.09	This work
LMP2	3.34		3.76	16.14		0.44	19.45	~ 2.3	[64]
PBEsol	3.33		3.07	14.57		0.34	16.42	~ 1.8	[64]
HF	3.33		7.71	21.64		1.87	23.40	~ 2.7	[64]
PBE-D	2.972		7.55	38.99		-3.20	57.50	~ 5.4	[64]
PBE0-D	2.956		10.91	44.01		-2.62	63.08	~ 6.2	[64]
PBE ( $d = 3.34 \text{ \AA}$ )			2.80	13.84		0.30	15.54	~ 2.0	[64]
PBE0 ( $d = 3.34 \text{ \AA}$ )			4.14	15.80		0.74	17.38	~ 1.8	[64]
PBE-D ( $d = 3.34 \text{ \AA}$ )			3.15	13.87		0.38	15.68	~ 1.9	[64]
PBE0-D ( $d = 3.34 \text{ \AA}$ )			4.49	15.83		0.90	17.45	~ 1.8	[64]
LDA	3.245		2	12		0	14		[93]
LDA	3.222		1.6	11.7		0.6	12.1		[97]

Table 6: Properties of hexagonal boron nitride bulk (for the layers aligned in the opposite directions: equilibrium interlayer distance  $d_{\text{eq}}$ , shear modulus  $C_{44}$ , modulus for axial compression  $C_{33}$ , frequencies of relative in-plane and out-of-plane vibrations  $f_E$  and  $f_B$ , respectively; for the layers aligned in the same direction: shear modulus  $C'_{44}$  and frequency of relative in-plane vibrations  $f'_E$ ) calculated using different functionals.

Approach	$d_{\text{eq}}$ (Å)	$C_{44}$ (GPa)	$C_{33}$ (GPa)	$f_E$ (cm <sup>-1</sup> )	$f_B$ (cm <sup>-1</sup> )	$C'_{44}$ (GPa)	$f'_E$ (cm <sup>-1</sup> )	Ref.
PBE-D2	3.088	8.62	63.40	64.58	175.17	9.08	66.29	This work
PBE-D3	3.398	3.96	27.90	41.71	110.76	3.72	40.42	This work
PBE-D3(BJ)	3.318	4.78	28.15	46.40	112.59	4.92	47.09	This work
PBE-TS	3.317	2.98	37.81	36.65	130.51	4.50	45.04	This work
PBE-TS/HI	3.386		26.93		109.01			This work
PBE-TS+SCS	3.326	2.93	36.45	36.27	127.99	3.71	40.82	This work
optPBE-vdW	3.388	3.91	29.71	41.52	114.47	3.76	40.74	This work
vdW-DF2	3.478	3.58	31.36	39.21	116.08	3.12	36.60	This work
PBE ( $d = d_{\text{exp}}$ )		5.21		48.56		5.09	47.99	This work
PBE-D2 ( $d = d_{\text{exp}}$ )		5.09		48.01		5.19	48.50	This work
PBE-D3 ( $d = d_{\text{exp}}$ )		5.47		49.75		5.34	49.16	This work
PBE-D3(BJ) ( $d = d_{\text{exp}}$ )		5.04		47.78		5.22	48.62	This work
PBE-TS ( $d = d_{\text{exp}}$ )		3.12		37.56		4.66	45.94	This work
PBE-TS+SCS ( $d = d_{\text{exp}}$ )		3.07		37.31		3.97	42.39	This work
optPBE-vdW ( $d = d_{\text{exp}}$ )		5.37		49.30		5.42	49.54	This work
vdW-DF2 ( $d = d_{\text{exp}}$ )		5.85		51.47		5.51	49.97	This work
LDA	3.08				120			[96]
LDA ( $d = 3.12$ Å)					90			[96]
PBE ( $d = 3.12$ Å)					122			[96]
EXX-RPA+	3.13				130 ± 10			[96]
Exp. 10 K	3.3013 ± 0.0010							[84]
Exp. 297.5 K	3.3265 ± 0.0010							[84]
Exp. 308.7 K	3.3300 ± 0.0005							[79]
Exp. 308.2 ± 0.5 K	3.3306 ± 0.0003							[80]
Exp. ~ 300 K	3.330 ± 0.004							[81–83]
Exp. ~ 300 K	3.341 ± 0.001							[87]
Exp. ~ 300 K	3.33 ± 0.02							[86]
Exp. ~ 300 K	3.329	7.7 ± 0.5	27.0 ± 0.5					[85]
Exp.	3.33							[117, 118]
Exp.	3.34–3.35	≤ 3						[119]
Exp.			32					[120]
Exp.				51.8				[121]
Exp.					125			[96]
Reference values	3.301	5.4	29.5	51.8	125			

ergies for graphene bilayer and graphite in the upper limit of the experimental range or even beyond it (Tables 1 and 2). To our knowledge no experimental data on the binding energy in boron nitride is available.

### 3.2. Potential energy surfaces

The characteristics of the potential energy surfaces are difficult to access from the experimental studies directly. Thus, we do not introduce in this case any reference values. However, the potential energy surfaces are important for understanding of the properties associated with relative motion of the layers. In the following we discuss principal features of the potential energy surfaces of graphene and hexagonal boron nitride and compare our results with the previous calculations.

In the case when boron nitride layers are aligned in the same direction the symmetry of the potential energy surface is the same as that of graphene (Fig. 1a and b) [54]. There are two equivalent energy minima AB in which half of the atoms of the adsorbed layer are located on top of the atoms of the bottom layer and the other half is on top of the hexagon centers. The saddle-point stacking SP that corresponds to the barrier to relative sliding of the layers is obtained by shifting the layers relative to each other by half of the bond length along the line connecting two adjacent minima AB. The maxima on the potential energy surface correspond to the AA stacking in which all atoms of the adsorbed layer are on top of the atoms of the bottom layer.

The barriers for relative sliding of the layers in graphene bilayer and graphite  $\Delta E_{SP} = E_{SP} - E_{AB}$  calculated using different functionals range from 0.75 meV/atom to 2.35 meV/atom (Tables 1 and 2), in agreement with the previously reported values of 0.5 – 2.1 meV/atom [43, 44, 50, 53, 55, 78]. The barriers obtained using the PBE-D2 and PBE-TS functionals are close to the estimates of the barrier from the experimental measurements of the shear mode frequency in bilayer, few-layer graphene and graphite of 1.7 meV/atom [51] and width of dislocations in few-layer graphene of 2.4 meV/atom [4], respectively. The magnitude of corrugation of the potential energy surface  $\Delta E_{AA} = E_{AA} - E_{AB}$  varies from 7.3 meV/atom to 20.4 meV/atom according to different functionals, in agreement with the values of 6 – 20 meV/atom obtained in previous DFT calculations [43, 44, 50, 53, 55, 78], 8.8 meV/atom from the RPA calculations [53] and  $\sim 12.4$  meV/atom from the QMC calculations [66] (Tables 1 and 2).

The barriers  $\Delta E_{SP}$  for bilayer and bulk boron nitride with the layers aligned in the same direction are in general slightly larger than the results for graphene and graphite

(Tables 1 and 2) and for most of the considered functionals range from 1.1 meV/atom to 2.0 meV/atom (Tables 3 and 5). The only exception is the PBE-D2 functional that gives too large barriers of 3.6 meV/atom and 4.2 meV/atom for bilayer and bulk boron nitride, respectively. As discussed below, this is the consequence of the small equilibrium interlayer distance for this functional. The LMP2 value of  $\sim 2.4$  meV/atom [64] and RPA value of 2.1 meV/atom [53] are below the PBE-D2 result but higher than the results obtained other considered functionals (Fig. 2). The calculated magnitudes of corrugation of the potential energy surface  $\Delta E_{AA}$  are 11 – 20 meV/atom for most of the functionals and 35 – 40 meV/atom for PBE-D2 (Tables 3 and 5). These values agree with the previously reported DFT data for boron nitride of 7 – 60 meV/atom [53, 64, 93, 97] as well as the LMP2 [64] (Fig. 2) and RPA [53] results of about 20 meV/atom and 11.4 meV/atom, respectively.

In the case of boron nitride with the layers aligned in the opposite directions, the potential energy surface has two inequivalent energy minima (Fig. 1c and d). The first energy minimum corresponds to the AA' stacking with all atoms of the adsorbed layer in the on-top position. The second energy minimum corresponds to the AB1' stacking in which the boron atoms of the adsorbed layer are on top of the boron atoms of the bottom layer and the nitrogen atoms are on top of the hexagon centers. The AB2' stacking with the nitrogen atoms in the on-top position and the boron atoms are on top of the hexagon centers has the maximal energy among all boron nitride stackings for the layers aligned in the opposite directions. The saddle-point stacking SP' corresponding to the barrier to relative sliding of the layers aligned in the opposite directions can be found by shifting the layers along the straight line corresponding to the transition between the AB1' and AA' stackings.

Almost all the considered functionals agree that the energies of the AA', AB1' and AB stackings of boron nitride layers are rather close and differ only by several meV/atom (Tables 3 and 5). However, the order of stability of these structures varies depending on the approach, which is supported by the literature data [47, 53, 64, 88, 93, 97]. While the experimental studies [79], RPA [53] and LMP2 [64] results and DFT calculations with account of nonlocal many-body dispersion (MBD) [122] suggest that the ground state of boron nitride corresponds to the AA' stacking, the most favourable stacking according to the PBE-D2 and PBE-D3(BJ) functionals is AB. The PBE-TS, PBE-TS/Hi and PBE-TS+SCS functionals predict that both the AB1' and AB stackings are lower in energy than

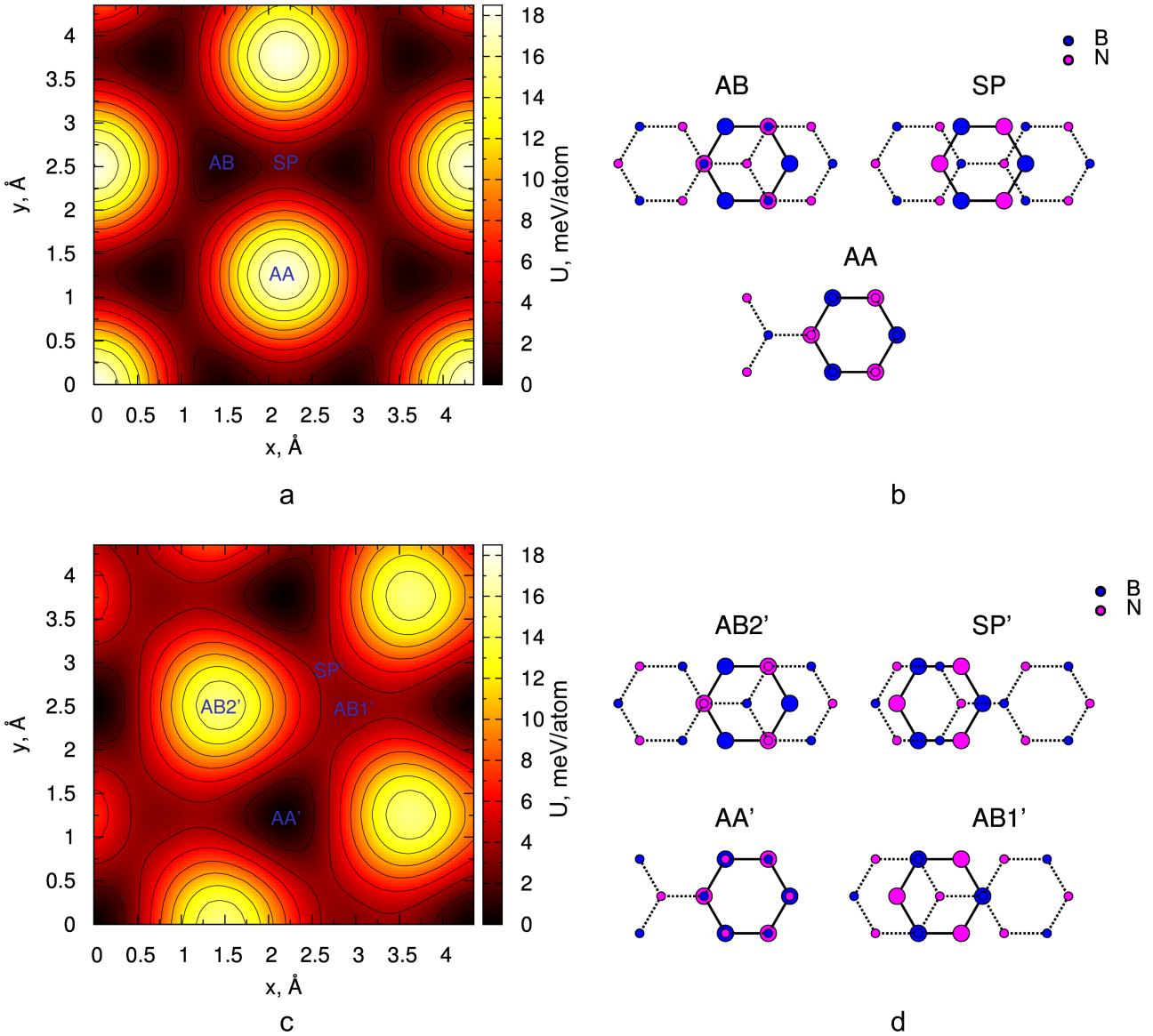


Figure 1: Interlayer interaction energy of hexagonal boron nitride bilayer  $U$  (in meV per atom of the top layer) as a function of the relative displacement of the layers in the armchair ( $x$ , in Å) and zigzag ( $y$ , in Å) directions calculated using the vdW-DF2 functional at the interlayer distance of  $d = 3.33$  Å: (a,b) boron nitride layers aligned in the same direction and (c,d) boron nitride layers aligned in the opposite directions. The energy is given relative to the AA' stacking. (b, d) Structures of the symmetric stackings are indicated. Boron and nitrogen atoms are coloured in blue and magenta, respectively.

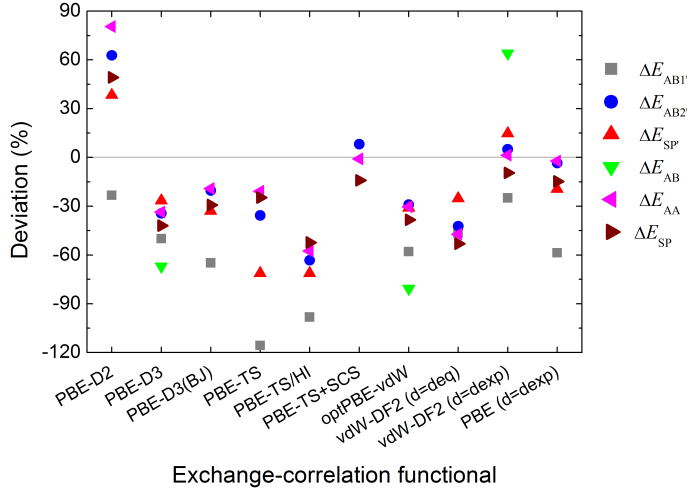


Figure 2: Relative deviation (in %) of the characteristics of the potential energy surface of hexagonal boron nitride bilayer calculated using different vdW-corrected exchange-correlation functionals at the equilibrium interlayer distance from the LMP2 data [64]: (squares)  $\Delta E_{AB1'} = E_{AB1'} - E_{AA'}$ , (circles)  $\Delta E_{AB2'} = E_{AB2'} - E_{AA'}$ , (triangles up)  $\Delta E_{SP'} = E_{SP'} - E_{AA'}$ , (triangles down)  $\Delta E_{AB} = E_{AB} - E_{AA'}$ , (triangles left)  $\Delta E_{AA} = E_{AA} - E_{AB}$  and (triangles right)  $\Delta E_{SP} = E_{SP} - E_{AB}$ . The results for the PBE functional without correction for vdW interactions are given for the experimental interlayer distance of  $d_{\text{exp}} = 3.30 \text{ \AA}$ . The results for the vdW-DF2 function are given both for the equilibrium ( $d = d_{\text{eq}}$ ) and experimental ( $d = d_{\text{exp}}$ ) interlayer distances. The data with deviation beyond -120% and 90% are not shown (see Table 3).

the AA stacking in boron nitride bulk (Table 5). For boron nitride bilayer, the PBE-TS functional gives the similar result, the PBE-TS/Hi shows the preference of the AB stacking over the AA' stacking, while according to the PBE-TS+SCS functional, the SP' and AB1' stackings strangely coincide and have the clearly overestimated relative energy of  $\Delta E_{AB1'} = E_{AB1'} - E_{AA'} = 8.6 \text{ meV/atom}$  (Table 3).

The only considered functionals that correctly describe the ground state of boron nitride are PBE-D3 and vdW-DF2. According to them, the energy difference between the AB and AA' stackings  $\Delta E_{AB} = E_{AB} - E_{AA'}$  is within 0.6 meV/atom, in agreement with the LMP2 [64] and RPA [53] results and the experimental data [115] that both the AA' and AB1' stackings can be observed for boron nitride bilayer. It should be nevertheless noted that the optPBE-vdW functional gives the correct order of stackings in energy for boron nitride bilayer, while for bulk the AB stacking is preferred over the AA' stacking only by 0.02 meV/atom, i.e. within the typical error of DFT calculations.

The barrier for transition from the AA' stacking to the AB1' one  $\Delta E_{SP'} = E_{SP'} - E_{AA'}$  varies for the PBE-D3, PBE-D3(BJ), optPBE-vdW and vdW-DF2 function-

als from 2.3 meV/atom to 2.9 meV/atom (Tables 3 and 5). The PBE-D2 functional gives remarkably higher values of 4.7 meV/atom and 5.6 meV/atom for boron nitride bilayer and bulk, respectively, while the PBE-TS and PBE-TS/Hi functionals predict the smaller values in the 0.6 – 1.0 meV/atom range. The PBE-TS+SCS functional provides the similarly small value of 0.7 meV/atom for the bulk material, while the result for bilayer of 8.6 meV/atom is clearly too large. For comparison, the LMP2 method gives the barrier for boron nitride bilayer of 3.4 meV/atom [64] (Fig. 2). The magnitudes of corrugation of the potential energy surface for boron nitride with the layers aligned in the opposite directions  $\Delta E_{AB2'} = E_{AB2'} - E_{AA'}$  range from 10 meV/atom to 30 meV/atom, similar to the values 7 – 44 meV/atom reported in literature for different DFT methods [53, 64, 93, 97] and including the LMP2 [64] and RPA [53] values of about 16 meV/atom and 11 meV/atom, respectively.

Clearly overestimated or underestimated corrugations of the potential energy surfaces obtained using different functionals can be attributed to too small or too large equilibrium interlayer distances. It is known from previous publications [44, 55] that the corrugations of the potential energy surface increase exponentially upon decreasing the interlayer distance  $d$ . Using the experimental interlayer distance of  $d_{\text{exp}} = 3.34 \text{ \AA}$  for graphene and graphite and  $d_{\text{exp}} = 3.30 \text{ \AA}$  for boron nitride, provides more reasonable values for characteristics of the potential energy surface for all the considered approaches except the DFT-TS family.

For graphene and graphite, the barrier  $\Delta E_{SP}$  and magnitude of corrugation  $\Delta E_{AA}$  obtained for the experimental interlayer distance using the PBE-D2, PBE-D3, PBE-D3(BJ), optPBE-vdW and vdW-DF2 functionals lie in the narrow ranges from 1.55 meV/atom to 1.65 meV/atom and from 13.7 meV/atom to 14.9 meV/atom, respectively (Tables 1 and 2). Therefore, using the equilibrium interlayer distance, the agreement with the estimate of the barrier from the experimental measurements of the shear mode frequency in bilayer, few-layer graphene and graphite of 1.7 meV/atom [51] is improved compared to the results for the equilibrium interlayer distance.

For boron nitride with the layers aligned in the same direction, the barrier  $\Delta E_{SP}$  and magnitude of corrugation  $\Delta E_{AA}$  obtained for the experimental interlayer distance using the PBE-D2, PBE-D3, PBE-D3(BJ), optPBE-vdW and vdW-DF2 functionals are 2.03 – 2.25 meV/atom and 19.0 – 20.0 meV/atom (Tables 3 and 5), respectively, in better agreement with the LMP2 values of  $\sim 2.4 \text{ meV/atom}$  and  $\sim 20 \text{ meV/atom}$  [64] (Fig. 2). For boron nitride with

the layers aligned in the opposite directions at the experimental interlayer distance, the characteristics  $\Delta E_{AB2'}$  and  $\Delta E_{SP'}$  are 15.9 – 17.5 meV/atom and 2.67 – 3.90 meV/atom, respectively. These values are also closer to the LMP2 data of 16.1 – 16.5 meV/atom and 3.4 meV/atom [64] (Fig. 2).

Therefore, the use of the experimental interlayer distance for most of the considered functionals improves the description of the potential energy surfaces both for graphite and boron nitride. This, however, does not solve the problem of the wrong ground-state stacking of boron nitride for the PBE-D2, PBE-D3(BJ) and optPBE-vdW functionals (Tables 3 and 5). In the case of the PBE-D3 functional the energy of the AB stacking of boron nitride bilayer relative to the AA' stacking also becomes slightly negative at the experimental interlayer distance. The functionals different from PBE, such as rPBE [123], revPBE [124] and PBEsol [125], in the pure form or with vdW corrections according to the DFT-D3 or DFT-D3(BJ) methods, suffer from the same deficiency. The use of the hybrid functionals, such as PBE0 [126], can be a solution (Table 3, these calculations were performed using the  $16 \times 24 \times 1$  k-point grid and the maximum kinetic energy of plane waves of 500 eV). Nevertheless, such functionals are heavy computationally. Among the considered standard functionals, vdW-DF2 is the only one that describes the order of the metastable states of boron nitride at the experimental interlayer distance both for bulk and bilayer. Moreover, using this approach, the relative energies of the AA', AB and AB1' stackings of hexagonal boron nitride are not just qualitatively correct but also quantitatively close to the results of the LMP2 calculations [64] (Tables 3 and 5, Fig. 2).

It should also be noted that the characteristics of the potential energy surfaces obtained at the experimental interlayer distances using the PBE-D2, PBE-D3, PBE-D3(BJ), optPBE-vdW and vdW-DF2 functionals are very close to those calculated using the PBE functional without any vdW correction (Tables 1–3 and 5). This is consistent with previous studies [44, 47, 50, 54, 55, 64], which suggest that the contribution of van der Waals interaction into the corrugation of the potential energy surface at a given interlayer distance is negligibly small. Similar observations hold also for the rPBE, revPBE and PBEsol functionals (Tables 3 and 5).

Let us now consider the difference in the characteristics of the potential energy surfaces  $\Delta E_{AB2'}$ ,  $\Delta E_{SP'}$ ,  $\Delta E_{AA}$  and  $\Delta E_{SP}$  for bilayer (Tables 1 and 3) and bulk (Tables 1 and 5) materials. This difference can be associated with the changes in the equilibrium interlayer distance and in-

teraction of non-adjacent layers in the bulk. Taking into account variation of the equilibrium interlayer distance, the differences in the listed properties for the PBE-D2, PBE-D3, PBE-D3(BJ), vdW-DF2 and optPBE-vdW functionals are within 20%. At the experimental interlayer distance only the effect of interaction of non-adjacent layers in the bulk is left and the differences in the characteristics of the potential energy surfaces are within 5%. Therefore, for these approaches, the effect of interaction of non-adjacent layers in bulk on the characteristics of the potential energy surface is much smaller compared to the changes in these characteristics due to variation of the equilibrium interlayer distance.

The much more prominent effect of non-adjacent layers is observed for the DFT-TS family of methods, especially for the DFT-TS+SCS approach, where the potential energy surfaces of boron nitride with the layers aligned in the opposite directions are qualitatively different for the bulk and bilayer materials. As mentioned above, according to this method, the SP' and AB1' stackings of the bilayer coincide and have a very high energy relative to the AA' stacking. Such a remarkable modification of the potential energy surface should be attributed to peculiarities of the screening effects in two-dimensional materials.

### 3.3. Frequencies and elastic properties

While the barrier to relative sliding of the layers and magnitude of the corrugation of the potential energy surfaces are difficult to measure directly, some information on the potential energy surfaces is contained in the available experimental data on the shear modulus  $C_{44}$  [28–32, 85, 119] and frequency  $f_E$  of the shear mode  $E_{2g}$  [29, 32, 37–39, 39, 40, 121]. The information describing the change of the binding energy with the interlayer distance corresponds to the modulus  $C_{33}$  for axial compression [28, 29, 32–36, 39, 85, 120] and frequency  $f_B$  of the out-of-plane  $B_{1g}$  mode [29, 36–38, 41, 42, 96]. As the reference data in these cases we use the average of the experimental values using that normally the experimental data fall within narrow intervals around the average values (Tables 2, 1 and 6). The error in the experimental measurements related to scatter of the data for graphite is within 9% and 13% for the moduli  $C_{33}$  [28, 29, 33–36] and  $C_{44}$  [28–32], respectively, and within 1% and 3% for the frequencies  $f_B$  [29, 36–38, 41] and  $f_E$  [29, 32, 37–40], respectively. The errors about 3% and 10% are associated with measurements of the frequencies  $f_B$  [41, 42] and  $f_E$  [32, 39] in graphene bilayer. For boron nitride, the experimental data are available only for bulk [85, 96, 119–121]. The errors related to scatter of the data for the moduli  $C_{44}$

[85, 119] and  $C_{33}$  [85, 120] are estimated as 40% and 8%, respectively.

In our calculations, the shear mode frequency  $f_E$  of bilayer in which the layers slide rigidly in the opposite in-plane directions is determined from the curvature  $\partial^2 U / \partial x^2$  of the potential energy surface for in-plane displacements out of a given energy minimum [51]

$$f_E = \frac{1}{2\pi} \sqrt{\frac{1}{\mu} \frac{\partial^2 U}{\partial x^2}}, \quad (7)$$

where  $\mu = m/2$  and  $m$  is the average mass of atoms in the layers. In bulk materials, the frequency is additionally multiplied by the factor of  $\sqrt{2}$  [51]. To find the curvature of the potential energy surface in-plane displacements up to 0.05 Å are considered along the armchair direction and the obtained energy curve is approximated by a parabola. For boron nitride, the calculations are performed for the AA' and AB stackings, which are very close in energy and can be both observed for bilayer [115]. Since the PBE-TS/Hi functional gives the non-parabolic dependences of potential energy on in-plane displacement around the AA' and AB stackings, we do not consider the properties characterizing relative in-plane motion of the layers in this case.

The same curvature  $\partial^2 U / \partial x^2$  of the potential energy surface also determines the shear modulus  $C_{44}$ , which has the same formula for bilayer and bulk

$$C_{44} = \frac{d}{\sigma} \frac{\partial^2 U}{\partial x^2}, \quad (8)$$

where  $\sigma = 3\sqrt{3}l^2/4$  is the area per atom ( $l$  is the bond length) and  $d$  is the interlayer distance.

The frequency  $f_B$  of relative out-of-plane vibrations of the layers and modulus for axial compression  $C_{33}$  are found by equations similar to eqs. 7 and 8 in which the curvature of the potential energy surface is taken for out-of-plane displacements  $\partial^2 U / \partial z^2$ . Out-of-plane displacements up to 0.5% of the equilibrium interlayer distance are considered and the obtained energy curve is approximated by a parabola. The accuracy of description of the elastic moduli and frequencies by different functionals is analyzed in detail in subsection 3.4.

### 3.4. Discussion

Let us first discuss the results of calculations in connection with the available experimental data for graphene bilayer and graphite (Tables 1 and 2, respectively). Deviations of the physical properties of graphene bilayer and graphite from the reference data obtained by averaging the

experimental values are shown in Fig. 3. It is seen that none of the functionals considered is able to reproduce these data fully. Similar discrepancies in the equilibrium lattice parameters, cohesive energy, interlayer binding energy, bulk modulus,  $C_{33}$  and  $C_{333}$  moduli and  $\pi_z$ -splitting of graphite were observed previously in Ref. [63].

The closest agreement with the reference data is achieved for the PBE-D2 approach. The functional gives the magnitude of the binding energy  $E_{AB}$  of graphite in the AB stacking at the upper limit of the experimental range (Table 2, 40% deviation from the reference value) and overestimates the shear modulus  $C_{44}$ , modulus  $C_{33}$  for axial compression and frequencies of relative in-plane  $f_E$  and out-of-plane  $f_B$  vibrations in graphene bilayer and graphite by 8–18%. The exaggeration of the characteristics related to in-plane displacement of the layers can be partially attributed to underestimation of the equilibrium interlayer distance  $d_{eq}$  by 3.4% and 2.8% in graphite and graphene bilayer, respectively. Though this deviation does not look large, the corrugations of the potential energy surface increase exponentially upon decreasing the interlayer distance  $d$  [44, 55]. Therefore, even a small deviation in the equilibrium interlayer distance  $d_{eq}$  results in a considerable error in the properties related to in-plane motion of the layers, such as the shear modulus  $C_{44}$  and shear mode frequency  $f_E$ . The underestimation of the equilibrium interlayer distance  $d_{eq}$  combined with overestimation of the binding energy  $E_{AB}$  can be responsible for overestimation of the properties related to out-of-plane motion of the layers including the modulus  $C_{33}$  for axial compression and the frequency  $f_B$  of out-of-plane vibrations.

Similar in magnitude deviations from the reference values are observed for the PBE-D3(BJ) functional (Fig. 3). The main difference from the PBE-D2 approach, however, is that the elastic moduli  $C_{44}$  and  $C_{33}$  and frequencies  $f_E$  and  $f_B$  are underestimated not overestimated. Such an underestimation for the properties  $C_{44}$  and  $f_E$  related to in-plane motion of the layers correlates with the overestimation of the equilibrium interlayer distance  $d_{eq}$  by 1.1% and 1.8% in graphite and graphene bilayer, respectively.

The PBE-TS functional reproduces very well the equilibrium interlayer distance  $d_{eq}$  (within 0.3%, Fig. 3) and the properties associated with in-plane relative displacement of the layers, the shear modulus  $C_{44}$  and shear mode frequency  $f_E$ , both for graphite and graphene bilayer (within 6%). However, it strongly overestimates the binding energy  $E_{AB}$  in graphite (by 105%), frequency  $f_B$  of relative out-of-plane vibrations and modulus  $C_{33}$  for axial compression (36% and 83% for graphite, respectively).

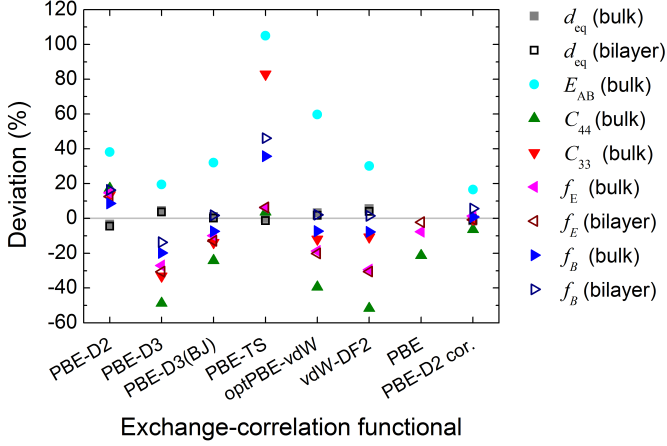


Figure 3: Relative deviation (in %) of the properties of graphite (filled symbols) and graphene bilayer (open symbols) calculated using different vdW-corrected exchange-correlation functionals from the reference experimental data: (squares) equilibrium interlayer distance  $d_{\text{eq}}$ , (circles) binding energy in the AB stacking  $E_{\text{AB}}$ , (triangles up) shear modulus  $C_{44}$ , (triangles down) modulus for axial compression  $C_{33}$ , (triangles left) shear mode frequency  $f_E$  and (triangles right) frequency of relative out-of-plane vibrations  $f_B$ . The results for the PBE functional without correction for vdW interactions are given for the experimental interlayer distance of  $d_{\text{exp}} = 3.34 \text{ \AA}$ .

The PBE-D3, vdW-DF2 and optPBE-vdW functionals noticeably overestimate the equilibrium interlayer distance  $d_{\text{eq}}$  (by 3–6%, Fig. 3). Correspondingly the shear mode frequencies  $f_E$  and shear modulus  $C_{44}$  are strongly underestimated (by 20–30% and 40–50%, respectively). Though the binding energy  $E_{\text{AB}}$  in graphite is within the experimental range (PBE-D3, vdW-DF2) or overestimated (optPBE-vdW), the frequency  $f_B$  of out-of-plane vibrations and modulus  $C_{33}$  for axial compression in graphite are underestimated (by 7–20% and 10–33%, respectively).

It is, however, premature to judge about the accuracy of different approaches on the basis of the results only for graphene bilayer and graphite. Indeed the comparison of the calculation results obtained using the PBE-D2 and PBE-TS functionals with the experimental data for hexagonal boron nitride bulk (Fig. 4) gives a picture very different from that for graphite. The equilibrium interlayer distance is much more underestimated by the PBE-D2 approach in boron nitride bulk (6.5%) compared to graphite (3.4%), which results in strongly overestimated properties related both to in-plane and out-of-plane relative motion of boron nitride layers (30–120%). The PBE-TS functional describes better the frequency  $f_B$  of relative out-of-plane vibrations and modulus  $C_{33}$  for axial compression (4.4% and 28% overestimation, respectively) compared to graphite but fails to reproduce the properties of boron nitride related to in-plane motion of the layers, the

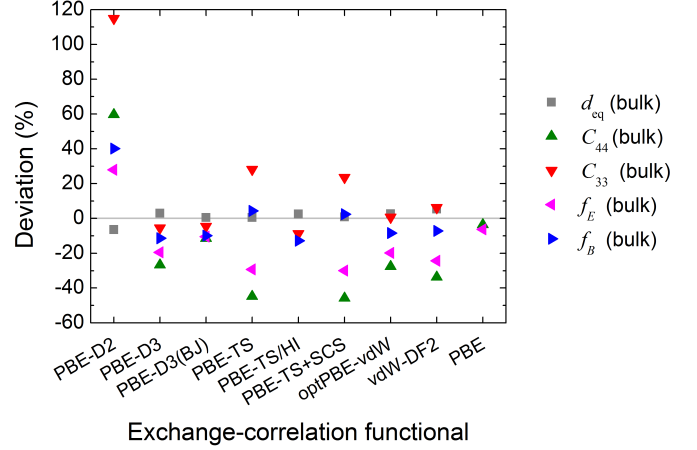


Figure 4: Relative deviation (in %) of the properties of hexagonal boron nitride bulk calculated using different vdW-corrected exchange-correlation functionals from the reference experimental data: (squares) equilibrium interlayer distance  $d_{\text{eq}}$ , (triangles up) shear modulus  $C_{44}$ , (triangles down) modulus for axial compression  $C_{33}$ , (triangles left) shear mode frequency  $f_E$  and (triangles right) frequency of relative out-of-plane vibrations  $f_B$ . The results for the PBE functional without correction for vdW interactions are given for the experimental interlayer distance of  $d_{\text{exp}} = 3.30 \text{ \AA}$ .

shear modulus  $C_{44}$  and shear mode frequency  $f_E$  (45% and 29% underestimation, respectively). Similar errors are observed in the properties characterizing relative in-plane motion of the layers for the PBE-TS+SCS functional, while evaluation of these quantities using the PBE-TS/Hi functional is complicated by the non-parabolic dependences of interlayer interaction energy on displacement around the AA' and AB stackings.

The PBE-D3, PBE-D3(BJ), optPBE-vdW and vdW-DF2 functionals give more consistent results in the calculations for graphite and boron nitride (Fig. 4). There is even some improvement for boron nitride. The closer approximation of the interlayer distance by these approaches in boron nitride relative to graphite is accompanied by the improved accuracy in the frequencies and moduli related both to in-plane and out-of-plane relative motion of the layers.

Based on the data both for graphite and boron nitride it can be concluded that the best description of the properties of the AB and AA' stackings, respectively, which are known to be the ground-state ones from the experimental studies, is provided by the PBE-D3(BJ) functional (Figs. 3 and 4). However, as discussed in subsection 3.2, this approach along with PBE-D2, PBE-TS, PBE-TS/Hi, PBE-TS+SCS and optPBE-vdW fails to predict the correct order in energy for the AA', AB1' and AB stackings of boron nitride. The functionals that adequately describe



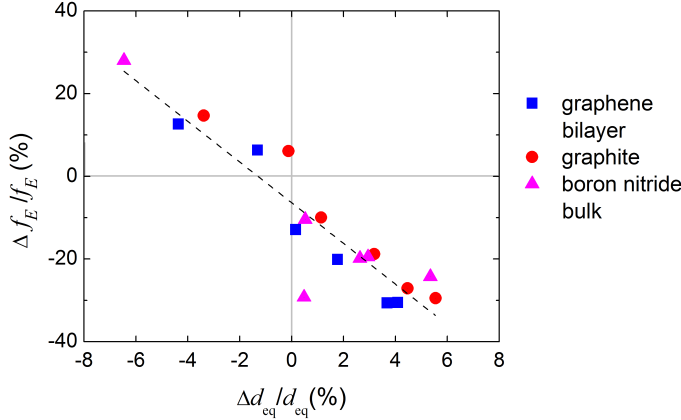


Figure 5: Calculated relative deviation  $\Delta f_E/f_E$  of the shear mode frequency (in %) as a function of the relative deviation  $\Delta d_{eq}/d_{eq}$  of the equilibrium interlayer distance (in %) for PBE-D2, PBE-D3, PBE-D3(BJ), PBE-TS, vdW-DF2 and optPBE-vdW functionals: (squares) graphene bilayer, (circles) graphite and (triangles) hexagonal boron nitride bulk. The dashed line corresponding to the linear approximation of the dependence is shown to guide the eye.

the relative stability of these metastable stackings, PBE-D3 and vdW-DF2, are comparable in accuracy (Figs. 3 and 4). The PBE-D3 functional is somewhat more precise in the properties associated with in-plane motion of the layers, the shear mode frequency  $f_E$  and shear modulus  $C_{44}$ , while the vdW-DF2 approach gives better results for the properties associated with out-of-plane motion of the layers, the frequency  $f_B$  of relative out-of-plane vibrations and modulus  $C_{33}$  for axial compression.

Considering only the latter group of properties, the results closest to the reference experimental data are obtained for three functionals: PBE-D3(BJ), optPBE-vdW and vdW-DF2. However, the use of the vdW-DF2 functional is preferred considering the correct ordering of the metastable states of hexagonal boron nitride in energy.

The comparison of the results obtained using the vdW-corrected functionals for graphene bilayer, graphite and boron nitride (Figs. 3 and 4) with the reference data suggests that the approaches that guess better the equilibrium interlayer distance are more precise for the properties associated with in-plane motion of the layers (Fig. 5). In fact, using the experimental interlayer distance for the PBE-D2, PBE-D3, PBE-D3(BJ), vdW-DF2 and optPBE-vdW functionals improves not only description of the characteristics of the potential energy surface, as discussed in section 3.2, but also of the shear moduli and shear mode frequencies (Tables 1 – 6).

The data obtained using these methods at the experimental interlayer distance are also very close to the results for the pure PBE functional without corrections for

vdW interactions (Tables 1 – 6). For the latter, the shear mode frequency  $f_E$  and shear modulus  $C_{44}$  of graphite calculated at the experimental interlayer distance are 7.7% and 21% below the reference data, respectively (Fig. 3). For graphene bilayer, the calculated shear mode frequency  $f_E$  is within the experimental range. For boron nitride, the shear mode frequency  $f_E$  and shear modulus  $C_{44}$  calculated at the experimental interlayer distance are 3.5% and 6.3% below the reference data, respectively (Fig. 4). Therefore, the use of the experimental interlayer distance seems to be appropriate for description of any properties related to in-plane relative displacement of the layers.

Again at the experimental interlayer distance most of the functionals including the pure PBE functional fail to describe the order of the metastable states of boron nitride in energy (Tables 3 and 5). Among the standard, i.e. non-hybrid, functionals, the correct relative energies of the metastable states of boron nitride both in the forms of bulk and bilayer are predicted in this case only by the vdW-DF2 functional. Thus this is the most adequate functional for calculations at the experimental interlayer distance.

It should be noted that agreement of the methods from the DFT-D family with the reference experimental data can be improved by readjustment of their semi-empirical parameters for specific materials. For example, the use of the dispersion coefficient  $C_6^C = 1.1725 \text{ J}\cdot\text{nm}^6/\text{mol}$  and van der Waals radius  $R_0^C = 1.4868 \text{ \AA}$  for carbon in the DFT-D2 approach (with  $s_6 = 1$ ) leads to much better description of the properties of graphene bilayer and graphite (see the results for the PBE-D2 corrected functional in Tables 1 and 2). In this case the relative deviation of the binding energy  $E_{AB}$  of graphite from the reference value is reduced to 16.5%, while the moduli  $C_{44}$  and  $C_{33}$  and frequencies  $f_E$  and  $f_B$  show the deviations within 6.5% (Fig. 3).

## 4. Conclusions

The DFT calculations of physical properties of bilayer graphene, graphite, bulk and bilayer boron nitride have been performed using different exchange-correlation functionals including corrections for vdW interactions. The performance of the functionals with respect to such experimentally measurable quantities as the equilibrium interlayer distance, binding energy, frequencies of relative in-plane and out-of-plane vibrations of the layers, shear modulus and modulus for axial compression has been compared.

It is shown that the best description of the listed properties for the AB stacking of graphene bilayer and graphite

and AA' stacking of boron nitride, which are known to be the ground-state ones from the experimental studies, is provided by the PBE-D3(BJ) functional. However, this approach fails to predict the order of the metastable states of boron nitride in energy. With account of this ordering, the best options are the PBE-D3 and vdW-DF2 functionals.

The properties associated with relative out-of-plane motion of the layers, the frequency of relative out-of-plane vibrations and modulus for axial compression, are especially relevant under external load. For these characteristics, the results of the PBE-D3(BJ), optPBE-vdW and vdW-DF2 functionals are the ones closest to the corresponding reference experimental data. The use of the vdW-DF2 functional is again preferred considering the correct ordering of the metastable states of boron nitride in energy.

Significant improvement in the properties related to in-plane relative motion of the layers, shear mode frequency and shear modulus, is achieved when the experimental equilibrium interlayer distance is used. In this case it is also recommended to use the vdW-DF2 functional, which adequately describes energetics of the metastable states of boron nitride. In addition, the use of the experimental equilibrium interlayer distance improves description of the characteristics of the potential energy surfaces, such as the barriers to relative sliding of the layers and magnitudes of corrugation, as compared to the available experimental estimates [51] and LMP2 data [64]. Therefore, such an approach is appropriate when it is needed to study the effects of structural defects or edges on in-plane relative motion or potential energy surfaces of the layers.

In the specific case of graphene and graphite, the PBE-D2 functional is found to work very well. Further improvement is achieved by using for carbon the dispersion coefficient  $C_6^C = 1.1725 \text{ J} \cdot \text{nm}^6/\text{mol}$  and van der Waals radius  $R_0^C = 1.4868 \text{ \AA}$ .

As for the comparison of the calculation results for bilayer and bulk materials, it is found that for most of the considered functionals (PBE-D2, PBE-D3, PBE-D3(BJ), optPBE-vdW and vdW-DF2) the interaction of non-adjacent layers in bulk has a much smaller effect on characteristics of the potential energy surface than the variation of the equilibrium interlayer distance.

## Acknowledgments

Authors acknowledge the computational time on the Multipurpose Computing Complex NRC "Kurchatov Institute". AL and AP acknowledge the Russian Foundation

for Basic Research (Grant 16-52-00181). IL acknowledges the financial support from Grupos Consolidados UPV/EHU del Gobierno Vasco (IT578-13) and EU-H2020 project "MOSTOPHOS" (n. 646259).

## References

## References

- [1] Z. Y. Rong, P. Kuiper, Electronic effects in scanning tunneling microscopy: Moiré pattern on a graphite surface, *Phys. Rev. B* 48 (1993) 17427–17431. doi:10.1103/PhysRevB.48.17427.
- [2] Y. Gan, W. Chu, L. Qiao, STM investigation on interaction between superstructure and grain boundary in graphite, *Surf. Sci.* 539 (2003) 120–128. doi:10.1016/S0039-6028(03)00786-6.
- [3] J. H. Warner, M. H. Rummeli, T. Gemming, B. Büchner, G. A. D. Briggs, Direct imaging of rotational stacking faults in few layer graphene, *Nano Lett.* 9 (2009) 102–106. doi:10.1021/nl8025949.
- [4] J. S. Alden, A. W. Tsen, P. Y. Huang, R. Hovden, L. Brown, J. Park, D. A. Muller, P. L. McEuen, Strain solitons and topological defects in bilayer graphene, *PNAS* 110 (2013) 11256–11260. doi:10.1073/pnas.1309394110.
- [5] L. Brown, R. Hovden, P. Huang, M. Wojcik, D. A. Muller, J. Park, Twinning and twisting of tri- and bilayer graphene, *Nano Lett.* 12 (2012) 1609–1615. doi:10.1021/nl204547v.
- [6] B. Butz, C. Dolle, F. Niekiel, K. Weber, D. Waldmann, H. B. Weber, B. Meyer, E. Spiecker, Dislocations in bilayer graphene, *Nature* 505 (2013) 533–537. doi:10.1038/nature12780.
- [7] J. Lin, W. Fang, W. Zhou, A. R. Lupini, J. C. Idrobo, J. Kong, S. J. Pennycook, S. T. Pantelides, AC/AB stacking boundaries in bilayer graphene, *Nano Letters* 13 (2013) 3262–3268. doi:10.1021/nl4013979.
- [8] M. Yankowitz, J. I.-J. Wang, A. G. Birdwell, Y.-A. Chen, K. Watanabe, T. Taniguchi, P. Jacquod, P. San-Jose, P. Jarillo-Herrero, B. J. LeRoy, Electric field control of soliton motion and stacking in trilayer graphene, *Nat. Mater.* 13 (2014) 786–789. doi:10.1038/nmat3965.
- [9] S. Hattendorf, A. Georgi, M. Liebmann, M. Morgenstern, Networks of ABA and ABC stacked graphene on mica observed by scanning tunneling microscopy, *Surf. Sci.* 610 (2013) 53–58. doi:10.1016/j.susc.2013.01.005.
- [10] P. San-Jose, R. V. Gorbachev, A. K. Geim, K. S. Novoselov, F. Guinea, Stacking boundaries and transport in bilayer graphene, *Nano Lett.* 14 (2014) 2052–2057. doi:10.1021/nl500230a.
- [11] B. Lalmi, J. C. Girard, E. Pallecchi, M. Silly, C. David, S. Latil, F. Sirotti, A. Ouerghi, Flower-shaped domains and wrinkles in trilayer epitaxial graphene on silicon carbide, *Sci. Rep.* 4 (2014) 4066. doi:10.1038/srep04066.
- [12] M. M. Benameur, F. Gargiulo, S. Manzeli, G. Autès, M. Tosun, O. V. Yazyev, A. Kis, Electromechanical oscillations in bilayer graphene, *Nat. Comm.* 6 (2015) 8582. doi:10.1038/ncomms9582.
- [13] L. Gong, R. J. Young, I. A. Kinloch, S. J. Haigh, J. H. Warner, J. A. Hinks, Z. Xu, L. Li, F. Ding, I. Riaz, R. Jalil, K. S. Novoselov, Reversible loss of bernal stacking during the deformation of few-layer graphene in nanocomposites, *ACS Nano* 7 (2013) 7287–7294. doi:10.1021/nn402830f.

- [14] M. Dienwiebel, G. S. Verhoeven, N. Pradeep, J. W. M. Frenken, J. A. Heimberg, H. W. Zandbergen, Superlubricity of graphite, *Phys. Rev. Lett.* 92 (2004) 126101. doi:10.1103/PhysRevLett.92.126101.
- [15] M. Dienwiebel, N. Pradeep, G. S. Verhoeven, H. W. Zandbergen, J. W. Frenken, Model experiments of superlubricity of graphite, *Surf. Sci.* 576 (2005) 197–211. doi:10.1016/j.susc.2004.12.011.
- [16] A. E. Filippov, M. Dienwiebel, J. W. M. Frenken, J. Klafter, M. Urbakh, Torque and twist against superlubricity, *Phys. Rev. Lett.* 100 (2008) 046102. doi:10.1103/PhysRevLett.100.046102.
- [17] I. V. Lebedeva, A. A. Knizhnik, A. M. Popov, O. V. Ershova, Y. E. Lozovik, B. V. Potapkin, Fast diffusion of a graphene flake on a graphene layer, *Phys. Rev. B* 82 (2010) 155460. doi:10.1103/PhysRevB.82.155460.
- [18] I. V. Lebedeva, A. A. Knizhnik, A. M. Popov, O. V. Ershova, Y. E. Lozovik, B. V. Potapkin, Diffusion and drift of graphene flake on graphite surface, *J. Chem. Phys.* 134 (2011) 104505. doi:10.1063/1.3557819.
- [19] Q. Zheng, B. Jiang, S. Liu, Y. Weng, L. Lu, Q. Xue, J. Zhu, Q. Jiang, S. Wang, L. Peng, Self-retracting motion of graphite microflakes, *Phys. Rev. Lett.* 100 (2008) 067205. doi:10.1103/PhysRevLett.100.067205.
- [20] A. M. Popov, I. V. Lebedeva, A. A. Knizhnik, Y. E. Lozovik, B. V. Potapkin, Molecular dynamics simulation of the self-retracting motion of a graphene flake, *Phys. Rev. B* 84 (2011) 245437. doi:10.1103/PhysRevB.84.245437.
- [21] R. Bistritzer, A. H. MacDonald, Transport between twisted graphene layers, *Phys. Rev. B* 81 (2010) 245412. doi:10.1103/PhysRevB.81.245412.
- [22] R. Bistritzer, A. H. MacDonald, Moiré bands in twisted double-layer graphene, *PNAS* 108 (2011) 12233–12237. doi:10.1073/pnas.1108174108.
- [23] N. A. Poklonski, A. I. Siahlo, S. A. Vyrko, A. M. Popov, Y. E. Lozovik, I. V. Lebedeva, A. A. Knizhnik, Graphene-based nanodynamometer, *J. Comp. Theor. Nanosci.* 10 (2013) 141–146. doi:10.1166/jctn.2013.2670.
- [24] K.-T. Lam, C. Lee, G. Liang, Bilayer graphene nanoribbon nanoelectromechanical system device: A computational study, *Appl. Phys. Lett.* 95 (2009) 143107. doi:10.1063/1.3243695.
- [25] Y. Qian, K.-T. Lam, C. Lee, G. Liang, The effects of interlayer mismatch on electronic properties of bilayer armchair graphene nanoribbons, *Carbon* 50 (2012) 1659–1666. doi:10.1016/j.carbon.2011.12.007.
- [26] J. Zheng, P. Guo, Z. Ren, Z. Jiang, J. Bai, Z. Zhang, Conductance fluctuations as a function of sliding motion in bilayer graphene nanoribbon junction: A first-principles investigation, *Appl. Phys. Lett.* 101 (2012) 083101. doi:10.1063/1.4739838.
- [27] K. K. Paulla, A. A. Farajian, Stacking stability, emergence of magnetization and electromechanical nanosensing in bilayer graphene nanoribbons, *J. Phys.: Cond. Matter* 25 (2013) 115303. doi:10.1088/0953-8984/25/11/115303.
- [28] A. Bosak, M. Krisch, M. Mohr, J. Maultzsch, C. Thomsen, Elasticity of single-crystalline graphite: Inelastic x-ray scattering study, *Phys. Rev. B* 75 (2007) 153408. doi:10.1103/PhysRevB.75.153408.
- [29] R. Nicklow, N. Wakabayashi, H. G. Smith, Lattice dynamics of pyrolytic graphite, *Phys. Rev. B* 5 (1972) 4951–4962. doi:10.1103/PhysRevB.5.4951.
- [30] M. Grimsditch, Shear elastic modulus of graphite, *J. Phys. C: Solid State Phys.* 16 (1983) L143–L144.
- [31] E. J. Seldin, C. W. Nezbeda, Elastic constants and electron-microscope observations of neutron-irradiated compression-annealed pyrolytic and single-crystal graphite, *J. Appl. Phys.* 41 (1970) 3389–3400. doi:10.1063/1.1659430.
- [32] P. H. Tan, W. P. Han, W. J. Zhao, Z. H. Wu, K. Chang, H. Wang, Y. F. Wang, N. Bonini, N. Marzari, N. Pugno, G. Savini, A. Lombardo, A. C. Ferrari, The shear mode of multilayer graphene, *Nat. Mater.* 11 (2012) 294–300. doi:10.1038/nmat3245.
- [33] O. L. Blakslee, D. G. Proctor, E. J. Seldin, G. B. Spence, T. Weng, Elastic constants of compression-annealed pyrolytic graphite, *J. Appl. Phys.* 41 (1970) 3373–3382. doi:10.1063/1.1659428.
- [34] W. B. Gauster, I. J. Fritz, Pressure and temperature dependences of the elastic constants of compression-annealed pyrolytic graphite, *J. Appl. Phys.* 45 (1974) 3309–3314. doi:10.1063/1.1663777.
- [35] N. Wada, R. Clarke, S. A. Solin, X-ray compressibility measurements of the graphite intercalates  $KC_8$  and  $KC_{24}$ , *Solid State Communications* 35 (1980) 675–679. doi:10.1016/0038-1098(80)90872-8.
- [36] B. Alzyab, C. H. Perry, C. Zahopoulos, O. A. Pringle, R. M. Nicklow, High-pressure neutron-scattering studies of graphite and stage-two graphite- $SbCl_5$ , *Phys. Rev. B* 38 (1988) 1544–1547. doi:10.1103/PhysRevB.38.1544.
- [37] M. Mohr, J. Maultzsch, E. Dobardžić, S. Reich, I. Milošević, M. Damnjanović, A. Bosak, M. Krisch, C. Thomsen, Phonon dispersion of graphite by inelastic x-ray scattering, *Phys. Rev. B* 76 (2007) 035439. doi:10.1103/PhysRevB.76.035439.
- [38] L. J. Brillson, E. Burnstein, A. A. Maradudin, T. Stark, in: D. L. Carter, R. T. Bate (Eds.), *Proceedings of the International Conference on Semimetals and Narrow Gap Semiconductors*, Pergamon Press, 1971, p. 187.
- [39] D. Boschetto, L. Malard, C. H. Lui, K. F. Mak, Z. Li, H. Yan, T. F. Heinz, Real-time observation of interlayer vibrations in bilayer and few-layer graphene, *Nano Lett.* 13 (2013) 4620–4623. doi:10.1021/nl401713h.
- [40] M. Hanfland, H. Beister, K. Syassen, Graphite under pressure: Equation of state and first-order Raman modes, *Phys. Rev. B* 39 (1989) 12598–12603. doi:10.1103/PhysRevB.39.12598.
- [41] C. H. Lui, T. F. Heinz, Measurement of layer breathing mode vibrations in few-layer graphene, *Phys. Rev. B* 87 (2013) 121404. doi:10.1103/PhysRevB.87.121404.
- [42] C. H. Lui, Z. Ye, C. Keiser, X. Xiao, R. He, Temperature-activated layer-breathing vibrations in few-layer graphene, *Nano Lett.* 14 (2014) 4615–4621. doi:10.1021/nl1501678j.
- [43] A. N. Kolmogorov, V. H. Crespi, Registry-dependent interlayer potential for graphitic systems, *Phys. Rev. B* 71 (2005) 235415. doi:10.1103/PhysRevB.71.235415.
- [44] I. V. Lebedeva, A. A. Knizhnik, A. M. Popov, Y. E. Lozovik, B. V. Potapkin, Interlayer interaction and relative vibrations of bilayer graphene, *Phys. Chem. Chem. Phys.* 13 (2011) 5687–5695. doi:10.1039/c0cp02614j.
- [45] I. Leven, I. Azuri, L. Kronik, O. Hod, Inter-layer potential for hexagonal boron nitride, *J. Chem. Phys.* 140 (2014) 104106. doi:10.1063/1.4867272.
- [46] I. Leven, T. Maaravi, I. Azuri, L. Kronik, O. Hod, Inter-layer potential for graphene/h-BN heterostructures, *J. Chem. Theor. Comp.* 12 (2016) 2896–2905. doi:10.1021/acs.jctc.6b00147.

- [47] N. Marom, J. Bernstein, J. Garel, A. Tkatchenko, E. Joselevich, L. Kronik, O. Hod, Stacking and registry effects in layered materials: The case of hexagonal boron nitride, *Phys. Rev. Lett.* 105 (2010) 046801. doi:10.1103/PhysRevLett.105.046801.
- [48] I. Leven, D. Krepel, O. Shemesh, O. Hod, Robust superlubricity in graphene/h-BN heterojunctions, *J. Phys. Chem. Lett.* 4 (2013) 115–120. doi:10.1021/jz301758c.
- [49] X. Zhao, L. Li, M. Zhao, Lattice match and lattice mismatch models of graphene on hexagonal boron nitride from first principles, *J. Phys. Condens. Matter* 26 (2014) 095002. doi:10.1088/0953-8984/26/9/095002.
- [50] O. V. Ershova, T. C. Lillestolen, E. Bichoutskaia, Study of polycyclic aromatic hydrocarbons adsorbed on graphene using density functional theory with empirical dispersion correction, *Phys. Chem. Chem. Phys.* 12 (2010) 6483–6491. doi:10.1039/C000370K.
- [51] A. M. Popov, I. V. Lebedeva, A. A. Knizhnik, Y. E. Lozovik, B. V. Potapkin, Barriers to motion and rotation of graphene layers based on measurements of shear mode frequencies, *Chem. Phys. Lett.* 536 (2012) 82–86. doi:10.1016/j.cpllett.2012.03.082.
- [52] I. V. Lebedeva, A. A. Knizhnik, A. M. Popov, Y. E. Lozovik, B. V. Potapkin, Modeling of graphene-based NEMS, *Physica E* 44 (2012) 949–954. doi:10.1016/j.physe.2011.07.018.
- [53] S. Zhou, J. Han, S. Dai, J. Sun, D. J. Srolovitz, Van der Waals bilayer energetics: Generalized stacking-fault energy of graphene, boron nitride, and graphene/boron nitride bilayers, *Phys. Rev. B* 92 (2015) 155438. doi:10.1103/PhysRevB.92.155438.
- [54] A. V. Lebedev, I. V. Lebedeva, A. A. Knizhnik, A. M. Popov, Interlayer interaction and related properties of bilayer hexagonal boron nitride: *ab initio* study, *RSC Advances* 6 (2016) 6423–6435. doi:10.1039/C5RA20882C.
- [55] M. Reguzzoni, A. Fasolino, E. Molinari, M. C. Righi, Potential energy surface for graphene on graphene: *Ab initio* derivation, analytical description, and microscopic interpretation, *Phys. Rev. B* 86 (2012) 245434. doi:10.1103/PhysRevB.86.245434.
- [56] S. Grimme, Semiempirical GGA-type density functional constructed with a long-range dispersion correction, *J. Comp. Chem.* 27 (2006) 1787–1799. doi:10.1002/jcc.20495.
- [57] S. Grimme, J. Antony, S. Ehrlich, H. Krieg, A consistent and accurate *ab initio* parametrization of density functional dispersion correction (DFT-D) for the 94 elements H-Pu, *J. Chem. Phys.* 132 (2010) 154104. doi:10.1063/1.3382344.
- [58] S. Grimme, S. Ehrlich, L. Goerigk, Effect of the damping function in dispersion corrected density functional theory, *J. Comp. Chem.* 32 (2011) 1456–1465. doi:10.1002/jcc.21759.
- [59] A. Tkatchenko, M. Scheffler, Accurate molecular van der Waals interactions from ground-state electron density and free-atom reference data, *Phys. Rev. Lett.* 102 (2009) 073005. doi:10.1103/PhysRevLett.102.073005.
- [60] M. Dion, H. Rydberg, E. Schröder, D. C. Langreth, B. I. Lundqvist, Van der Waals density functional for general geometries, *Phys. Rev. Lett.* 92 (2004) 246401. doi:10.1103/PhysRevLett.92.246401.
- [61] K. Lee, E. D. Murray, L. Kong, B. I. Lundqvist, D. C. Langreth, Higher-accuracy van der Waals density functional, *Phys. Rev. B* 82 (2010) 081101. doi:10.1103/PhysRevB.82.081101.
- [62] J. Klimeš, D. R. Bowler, A. Michaelides, Chemical accuracy for the van der Waals density functional, *J. Phys.: Condens. Matter* 22 (2010) 022201. doi:10.1088/0953-8984/22/2/022201.
- [63] C. R. C. Rêgo, L. N. Oliveira, P. Tereshchuk, J. L. F. Da Silva, Comparative study of van der Waals corrections to the bulk properties of graphite, *J. Phys.: Condens. Matter* 27 (2016) 415502. doi:10.1088/0953-8984/27/41/415502.
- [64] G. Constantinescu, A. Kuc, T. Heine, Stacking in bulk and bilayer hexagonal boron nitride, *Phys. Rev. Lett.* 111 (2013) 036104. doi:10.1103/PhysRevLett.111.036104.
- [65] S. Lebègue, J. Harl, T. Gould, J. G. Ángyán, G. Kresse, J. F. Dobson, Cohesive properties and asymptotics of the dispersion interaction in graphite by the random phase approximation, *Phys. Rev. Lett.* 105 (2010) 196401. doi:10.1103/PhysRevLett.105.196401.
- [66] E. Mostaani, N. D. Drummond, V. I. Fal’ko, Quantum Monte Carlo calculation of the binding energy of bilayer graphene, *Phys. Rev. Lett.* 115 (2015) 115501. doi:10.1103/PhysRevLett.115.115501.
- [67] L. Spanu, S. Sorella, G. Galli, Nature and strength of interlayer binding in graphite, *Phys. Rev. Lett.* 103 (2009) 196401. doi:10.1103/PhysRevLett.103.196401.
- [68] G. Kresse, J. Furthmüller, Efficient iterative schemes for *ab initio* total-energy calculations using a plane-wave basis set, *Phys. Rev. B* 54 (1996) 11169–11186. doi:10.1103/PhysRevB.54.11169.
- [69] G. Kresse, D. Joubert, From ultrasoft pseudopotentials to the projector augmented-wave method, *Phys. Rev. B* 59 (1999) 1758–1775. doi:10.1103/PhysRevB.59.1758.
- [70] H. J. Monkhorst, J. D. Pack, Special points for Brillouin-zone integrations, *Phys. Rev. B* 13 (1976) 5188–5192. doi:10.1103/PhysRevB.13.5188.
- [71] J. P. Perdew, K. Burke, M. Ernzerhof, Generalized gradient approximation made simple, *Phys. Rev. Lett.* 77 (1996) 3865–3868. doi:10.1103/PhysRevLett.77.3865.
- [72] J. D. Bernal, The structure of graphite, *Proc. R. Soc. London, Ser. A* 106 (1924) 749–773. doi:10.1098/rspa.1924.0101.
- [73] V. Baskin, L. Meyer, Lattice constants of graphite at low temperatures, *Phys. Rev.* 100 (1955) 544. doi:10.1103/PhysRev.100.544.
- [74] R. W. Lynch, H. G. Drickamer, Effect of high pressure on the lattice parameters of diamond, graphite, and hexagonal boron nitride, *J. Chem. Phys.* 44 (1966) 181–184. doi:10.1063/1.1726442.
- [75] V. A. Ludsteck, Bestimmung der Änderung der Gitterkonstanten und des anisotropen Debye-Waller-faktors von Graphit mittels Neutronenbeugung im Temperaturbereich von 25 bis 1850° C, *Acta Crystallographica, Section A* 28 (1972) 59–65. doi:10.1107/S0567739472000130.
- [76] P. Trucano, R. Chen, Structure of graphite by neutron diffraction, *Nature* 258 (1975) 136–137. doi:10.1038/258136a0.
- [77] Y. X. Zhao, I. L. Spain, X-ray diffraction data for graphite to 20 GPa, *Phys. Rev. B* 40 (1989) 993–997. doi:10.1103/PhysRevB.40.993.
- [78] M. Aoki, H. Amawashi, Dependence of band structures on stacking and field in layered graphene, *Solid State Communications* 142 (2007) 123–127. doi:10.1016/j.ssc.2007.02.013.
- [79] R. S. Pease, Crystal structure of boron nitride, *Nature* 165 (1950) 722–723. doi:10.1038/165722b0.
- [80] R. S. Pease, An X-ray study of boron nitride, *Acta Crystallographica* 5 (1952) 356–361. doi:10.1107/S0365110X52001064.
- [81] V. L. Solozhenko, G. Will, F. Elf, Isothermal compres-

- sion of hexagonal graphite-like boron nitride up to 12 GPa, *Solid State Communications* 96 (1995) 1–3. doi:10.1016/0038-1098(95)00381-9.
- [82] V. L. Solozhenko, T. Peun, Compression and thermal expansion of hexagonal graphite-like boron nitride up to 7 GPa and 1800 K, *J. Phys. Chem. Solids* 58 (1997) 1321–1323. doi:10.1016/S0022-3697(97)00037-1.
- [83] V. L. Solozhenko, A. G. Lazarenko, J.-P. Petitet, A. V. Kanaev, Bandgap energy of graphite-like hexagonal boron nitride, *J. Phys. Chem. Solids* 62 (2001) 1331–1334. doi:10.1016/S0022-3697(01)00030-0.
- [84] W. Paszkowicz, J. B. Pelka, M. Knapp, T. Szyszko, S. Podsiadlo, Lattice parameters and anisotropic thermal expansion of hexagonal boron nitride in the 10 – 297.5 K temperature range, *Appl. Phys. A* 75 (2002) 431–435. doi:10.1007/s003390100999.
- [85] A. Bosak, J. Serrano, M. Krisch, K. Watanabe, T. Taniguchi, H. Kanda, Elasticity of hexagonal boron nitride: Inelastic x-ray scattering measurements, *Phys. Rev. B* 73 (2006) 041402. doi:10.1103/PhysRevB.73.041402.
- [86] K. Fuchizaki, T. Nakamichi, H. Saitoh, Y. Katayama, Equation of state of hexagonal boron nitride, *Solid State Communications* 148 (2008) 390–394. doi:10.1016/j.ssc.2008.09.031.
- [87] C. S. Yoo, J. Akella, H. Cynn, M. Nicol, Direct elementary reactions of boron and nitrogen at high pressures and temperatures, *Phys. Rev. B* 56 (1997) 140–146. doi:10.1103/PhysRevB.56.140.
- [88] A. Nag, K. Raidongia, K. P. S. S. Hembram, R. Datta, U. V. Waghmare, C. N. R. Rao, Graphene analogues of BN: Novel synthesis and properties, *ACS Nano* 4 (2010) 1539–1544. doi:10.1021/nn9018762.
- [89] K. Albe, Theoretical study of boron nitride modifications at hydrostatic pressures, *Phys. Rev. B* 55 (1997) 6203–6210. doi:10.1103/PhysRevB.55.6203.
- [90] G. Kern, G. Kresse, J. Hafner, *Ab initio* calculation of the lattice dynamics and phase diagram of boron nitride, *Phys. Rev. B* 59 (1999) 8551–8559. doi:10.1103/PhysRevB.59.8551.
- [91] N. Ohba, K. Miwa, N. Nagasako, A. Fukumoto, First-principles study on structural, dielectric, and dynamical properties for three BN polytypes, *Phys. Rev. B* 63 (2001) 115207. doi:10.1103/PhysRevB.63.115207.
- [92] A. Janotti, S.-H. Wei, D. J. Singh, First-principles study of the stability of BN and C.
- [93] L. Liu, Y. P. Feng, Z. X. Shen, Structural and electronic properties of h-BN, *Phys. Rev. B* 68 (2003) 104102. doi:10.1103/PhysRevB.68.104102.
- [94] H. Rydberg, M. Dion, N. Jacobson, E. Schröder, P. Hyldgaard, S. I. Simak, D. C. Langreth, B. I. Lundqvist, Van der Waals density functional for layered structures, *Phys. Rev. Lett.* 91 (2003) 126402. doi:10.1103/PhysRevLett.91.126402.
- [95] T. Tohei, A. Kuwabara, F. Oba, I. Tanaka, Debye temperature and stiffness of carbon and boron nitride polymorphs from first principles calculations, *Phys. Rev. B* 73 (2006) 064304. doi:10.1103/PhysRevB.73.064304.
- [96] A. Marini, P. García-González, A. Rubio, First-principles description of correlation effects in layered materials, *Phys. Rev. Lett.* 96 (2006) 136404. doi:10.1103/PhysRevLett.96.136404.
- [97] N. Ooi, V. Rajan, J. Gottlieb, Y. Catherine, J. B. Adams, Structural properties of hexagonal boron nitride.
- [98] J. Serrano, A. Bosak, R. Arenal, M. Krisch, K. Watanabe, T. Taniguchi, H. Kanda, A. Rubio, L. Wirtz, Vibrational properties of hexagonal boron nitride: Inelastic x-ray scattering and *ab initio* calculations, *Phys. Rev. Lett.* 98 (2007) 095503. doi:10.1103/PhysRevLett.98.095503.
- [99] I. Hamdi, N. Meskini, *Ab initio* study of the structural, elastic, vibrational and thermodynamic properties of the hexagonal boron nitride: Performance of LDA and GGA, *Physica B* 405 (2010) 2785–2794. doi:10.1016/j.physb.2010.03.070.
- [100] C. Adamo, V. Barone, Toward reliable density functional methods without adjustable parameters: The PBE0 model, *J. Chem. Phys.* 110 (1999) 6158–6170. doi:10.1063/1.478522.
- [101] H. B. G. Casimir, D. Polder, The influence of retardation on the London-van der Waals forces, *Phys. Rev.* 73 (1948) 360–372. doi:10.1103/PhysRev.73.360.
- [102] T. Bučko, S. Lebègue, J. Hafner, J. G. Ángyán, Improved density dependent correction for the description of London dispersion forces, *J. Chem. Theor. Comput.* 9 (2013) 4293–4299. doi:10.1021/ct400694h.
- [103] T. Bučko, S. Lebègue, J. G. Ángyán, J. Hafner, Extending the applicability of the Tkatchenko-scheffler dispersion correction via iterative hirshfeld partitioning, *J. Chem. Phys.* 141 (2014) 034114. doi:10.1063/1.4890003.
- [104] P. Bultinck, C. Van Alsenoy, P. W. Ayers, R. Carbó-Dorca, Critical analysis and extension of the Hirshfeld atoms in molecules, *J. Chem. Phys.* 126 (2007) 144111. doi:10.1063/1.2715563.
- [105] A. Tkatchenko, R. A. DiStasio, R. Car, M. Scheffler, Accurate and efficient method for many-body van der Waals interactions, *Phys. Rev. Lett.* 108 (2012) 236402. doi:10.1103/PhysRevLett.108.236402.
- [106] J. Klimeš, D. R. Bowler, A. Michaelides, Van der Waals density functionals applied to solids, *Phys. Rev. B* 83 (2011) 195131. doi:10.1103/PhysRevB.83.195131.
- [107] X. Weng, J. A. Robinson, K. Trumbull, R. Cavalero, M. A. Fanton, D. Snyder, Structure of few-layer epitaxial graphene on 6H-SiC (0001) at atomic resolution, *Appl. Phys. Lett.* 97 (2010) 201905. doi:10.1063/1.3517505.
- [108] F. Varchon, R. Feng, J. Hass, X. Li, B. Ngoc Nguyen, C. Naud, P. Mallet, J. Veuillen, C. Berger, E. H. Conrad, L. Magaud, Electronic structure of epitaxial graphene layers on SiC: Effect of the substrate, *Phys. Rev. Lett.* 99 (2007) 126805. doi:10.1103/PhysRevLett.99.126805.
- [109] D. Zhu, H. Gao, X. Zhang, T. Yang, L. Li, G. Yin, X. Li, C. Nicklin, X. Gao, Z. Li, L. Yi, X. Li, Real-time observation of graphene layer growth: Coupling of the interlayer spacing with thickness, *Carbon* 94 (2015) 775–780. doi:10.1016/j.carbon.2015.07.047.
- [110] Y. K. Koh, M.-H. Bae, D. G. Cahill, E. Pop, Reliably counting atomic planes of few-layer graphene ( $n > 4$ ), *ACS Nano* 5 (2011) 269–274. doi:10.1021/nn102658a.
- [111] R. Zacharia, H. Ulbricht, T. Hertel, Interlayer cohesive energy of graphite from thermal desorption of polyaromatic hydrocarbons, *Phys. Rev. B* 69 (2004) 155406. doi:10.1103/PhysRevB.69.155406.
- [112] L. A. Girifalco, R. A. Lad, Energy of cohesion, compressibility, and the potential energy functions of the graphite system, *J. Chem. Phys.* 25 (1956) 693–696. doi:10.1063/1.1743030.
- [113] L. X. Benedict, N. G. Chopra, M. L. Cohen, A. Zettl, S. G. Louie, V. H. Crespi, Microscopic determination of the interlayer binding energy in graphite, *Chem. Phys. Lett.* 286 (1998) 490–496. doi:10.1016/S0009-2614(97)01466-8.
- [114] Z. Liu, J. Z. Liu, Y. Cheng, Z. Li, L. Wang, Q. Zheng, Interlayer

- binding energy of graphite: A mesoscopic determination from deformation, *Phys. Rev. B* 85 (2012) 205418. doi:10.1103/PhysRevB.85.205418.
- [115] J. H. Warner, M. H. Rummeli, A. Bachmatiuk, B. Büchner, Atomic resolution imaging and topography of boron nitride sheets produced by chemical exfoliation, *ACS Nano* 4 (2010) 1299–1304. doi:10.1021/nn901648q.
- [116] C. Zhi, Y. Bando, C. Tang, H. Kuwahara, D. Golberg, Large-scale fabrication of boron nitride nanosheets and their utilization in polymeric composites with improved thermal and mechanical properties, *Adv. Mater.* 21 (2009) 2889 – 2893. doi:10.1002/adma.200900323.
- [117] Y. Kobayashi, T. Nakamura, T. Akasaka, T. Makimoto, N. Matsumoto, Hexagonal boron nitride on Ni(111) substrate grown by flow-rate modulation epitaxy, *Journal of Crystal Growth* 298 (2007) 325–327. doi:10.1016/j.jcrysgro.2006.10.034.
- [118] Y. Kobayashi, T. Akasaka, T. Makimoto, Hexagonal boron nitride grown by MOVPE, *Journal of Crystal Growth* 310 (2008) 5048–5052. doi:10.1016/j.jcrysgro.2008.07.057.
- [119] L. Duclaux, B. Nysten, J.-P. Issi, A. W. Moore, Structure and low-temperature thermal conductivity of pyrolytic boron nitride, *Phys. Rev. B* 46 (1992) 3362–3367. doi:10.1103/PhysRevB.46.3362.
- [120] B. Jager, Ph.D. thesis, Université de Grenoble, Grenoble, 1977.
- [121] R. J. Nemanich, S. A. Solin, R. M. Martin, Light scattering study of boron nitride microcrystals, *Phys. Rev. B* 23 (1981) 6348–6356. doi:10.1103/PhysRevB.23.6348.
- [122] W. Gao, A. Tkatchenko, Sliding mechanisms in multilayered hexagonal boron nitride and graphene: The effects of directionality, thickness, and sliding constraints, *Phys. Rev. Lett.* 114 (2015) 096101. doi:10.1103/PhysRevLett.114.096101.
- [123] B. Hammer, L. B. Hansen, J. K. Nørskov, Improved adsorption energetics within density-functional theory using revised Perdew-Burke-Ernzerhof functionals, *Phys. Rev. B* 59 (1999) 7413–7421. doi:10.1103/PhysRevB.59.7413.
- [124] Y. Zhang, W. Yang, Comment on “Generalized gradient approximation made simple”, *Phys. Rev. Lett.* 80 (1998) 890. doi:10.1103/PhysRevLett.80.890.
- [125] J. P. Perdew, A. Ruzsinszky, G. I. Csonka, O. A. Vydrov, G. E. Scuseria, L. A. Constantin, X. Zhou, K. Burke, Restoring the density-gradient expansion for exchange in solids and surfaces, *Phys. Rev. Lett.* 100 (2008) 136406. doi:10.1103/PhysRevLett.100.136406.
- [126] J. P. Perdew, M. Ernzerhof, K. Burke, Rationale for mixing exact exchange with density functional approximations, *J. Chem. Phys.* 105 (1996) 9982–9985. doi:10.1063/1.472933.